machines

MDPI

Article

Multi-Objective Optimization of the Grinding Process in a Spring-Rotor Mill Using Regression-Based Modeling

Aidos Baigunusov [1], Bekbolat Moldakhanov [1,2], Alina Kim [1,3,*], Mikhail Doudkin [1,2], Vladimir Yakovlev [1], Piotr Stryczek [4] and Tadeusz Lesniewski [4]

[1] International School of Engineering, D. Serikbayev East Kazakhstan Technical University, Ust-Kamenogorsk 070004, Kazakhstan; foraiphone207@gmail.com (A.B.); bekmoldahanov35@gmail.com (B.M.); mdudkin@ektu.kz (M.D.); vyakovlev@ektu.kz (V.Y.)
[2] LLP Europlus Vostok, Ust-Kamenogorsk 070000, Kazakhstan
[3] Miras University, Shymkent 160000, Kazakhstan
[4] Faculty of Mechanical Engineering, Wroclaw University of Science and Technology, 50-370 Wroclaw, Poland; piotr.stryczek@pwr.edu.pl (P.S.); tadeusz.lesniewski@pwr.edu.pl (T.L.)
* Correspondence: alinakim3107@gmail.com; Tel.: +7-777-496-73-10

Abstract

This study addresses the problem of improving the efficiency of fine grinding of bulk materials in a spring-rotor mill. The objective is to determine technologically sound operating parameters based on mathematical modeling, design of experiments, and multi-objective optimization. The methodology relies on a full-factorial experimental design according to the Hartley plan, with five control factors: rotor rotational speed, material loading ratio, overlap of the working zones, grinding chamber clearance, and grinding duration. The analyzed responses include grinding fineness, throughput, power consumption, specific energy consumption, and specific metal intensity. Based on experimental data, adequate second-order polynomial regression models were obtained for all response variables using the least-squares method. Statistical analysis showed that grinding time and rotational speed had the most significant influence on the process. Multi-objective optimization using the weighted-sum method enabled the identification of optimal operating conditions that balance product quality, throughput, and energy consumption. Verification experiments confirmed the adequacy of the developed models. Practical implementation of the optimized regimes increases throughput by 15–20% while simultaneously reducing energy consumption by 8–12% compared with empirically selected operating conditions. The proposed models and recommendations provide a quantitative basis for tuning and controlling grinding equipment in processing industries.

Keywords: grinding; spring-rotor mill; design of experiments; regression modeling; multi-objective optimization; weighted-sum method; Pareto front; energy efficiency

Check for updates

Academic Editor: António Pereira

Received: 23 February 2026
Revised: 17 March 2026
Accepted: 20 March 2026
Published: 23 March 2026

Copyright: © 2026 by the authors. Licensee MDPI, Basel, Switzerland. This article is an open access article distributed under the terms and conditions of the Creative Commons Attribution (CC BY) license.

1. Introduction

1.1. Industrial Significance of Grinding Processes

Grinding of bulk materials is one of the most energy-intensive and technologically critical operations in the processing chains of the mining, chemical, construction, metallurgical, pharmaceutical, and agricultural industries. The efficiency of grinding processes directly determines product quality, production cost, and the overall energy footprint of industrial plants [1–3]. According to comprehensive studies, comminution processes account for a significant portion of global energy consumption, with particularly high shares in mining

and mineral processing operations [1,2]. In the cement industry, for example, grinding consumes the majority of the total electrical energy required for production [3].

Under increasingly stringent environmental regulations and rising energy prices, the intensification and optimization of comminution processes have become a key engineering challenge. Improving energy efficiency in comminution could result in substantial global energy savings, equivalent to the annual electricity consumption of millions of households [3]. Furthermore, the growing demand for fine and ultra-fine powders in advanced materials, pharmaceuticals, and high-performance composites necessitates the development of more efficient grinding technologies and optimization methodologies [4–6].

1.2. Spring-Rotor Mills: Principles and Potential

Spring-rotor mills represent a promising class of equipment for fine grinding and waste processing, offering high specific throughput, relatively low energy consumption, and compact design compared to conventional ball, rod, or hammer mills [4–6]. The fundamental operating principle of these devices involves the combined action of multiple fracture mechanisms: impact loading in a centrifugal force field, compressive crushing against the chamber walls, and intensive abrasion in the engagement zone of counter-rotating rotors equipped with elastic spring elements or brackets (Figure 1).

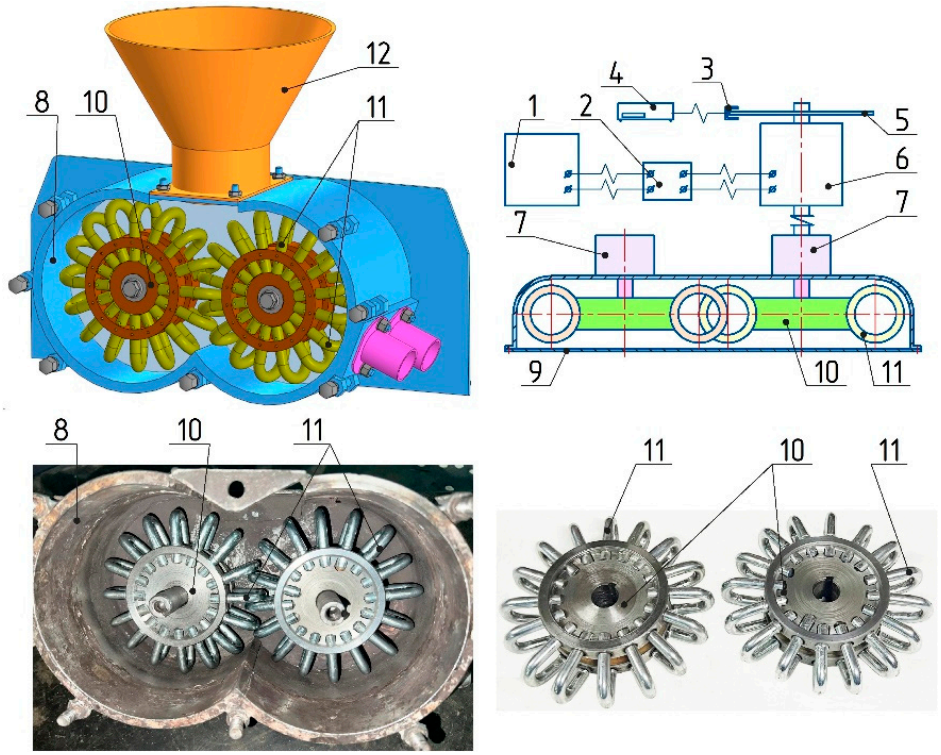


Figure 1. Schematic diagram of the single-row experimental test bench: (1) power supply; (2) wattmeter; (3) tachometer sensor; (4) tachometer; (5) disk; (6) drive electric motor; (7) bearing supports; (8) housing; (9) front wall; (10) rotor disk; (11) working element; (12) feed hopper.

The unique advantage of spring-rotor mills lies in their ability to generate high-intensity stress fields within a relatively small volume through the elastic deformation and recovery of spring elements. Unlike rigid impactors, spring elements store and release energy cyclically, creating pulsating loads that promote inter-particle comminution and reduce the risk of over-grinding [4,5]. This characteristic makes them particularly suitable for processing brittle materials, industrial wastes, and fibrous substances where conventional mills often exhibit poor efficiency or rapid wear [6,7].

However, the technological performance of spring-rotor mills is governed by a complex nonlinear interaction of multiple design and operating parameters that are strongly interdependent. These include rotational speed, material filling ratio, geometric configuration of rotors (overlap and clearance), and grinding duration. The optimization of such systems through conventional empirical tuning approaches is substantially limited by the inability to account for parameter interactions and the multi-objective nature of performance requirements [8–13].

1.3. Historical Development and State of the Art in Spring-Rotor Mill Research

The concept of utilizing spring elements as working bodies in grinding equipment has evolved over several decades, with significant contributions from research groups worldwide.

1.3.1. Pioneering Work by Sivachenko and Colleagues

The foundational research on spring-based grinding devices was conducted by Sivachenko and his research team [4,7]. Their pioneering work, patented in the United States (US Patent 4,899,941) and other countries, introduced the concept of mills with open-coil spring working elements operating within a closed tubular housing [4]. In these devices, springs are bent inside the housing, and material comminution occurs through alternating inter-coil spaces that change as the spring rotates. Sivachenko's research demonstrated that such configurations provide effective capture and fragmentation of material particles through combined impact, shear, and abrasion loads [4,7].

Subsequent studies established fundamental relationships between spring parameters (diameter, pitch, wire thickness) and mill performance characteristics. They also developed mathematical models for power consumption in spring mills, decomposing total power into components related to material fracture, internal friction, material transport, rolling resistance between coils, and material–wall friction [4,7]. However, their work primarily focused on qualitative performance assessment and mechanical behavior, with limited attention to systematic quantitative optimization.

1.3.2. Mechanical Analysis and Dynamic Behavior

The dynamic behavior and reliability of spring working elements under complex loading conditions have been systematically investigated by Sorokin, Zhou, and colleagues [5,10,12,13]. Using advanced finite element analysis and experimental validation, Sorokin and Zhou [5] developed rational calculation methods for spring mechanisms subjected to combined bending and torsion. They proposed a finite element in the form of a single coil turn that accounts for shear deformation and rotary inertia, enabling accurate prediction of natural frequencies and mode shapes of helical springs.

Badikov and Sorokin [13] experimentally validated critical torque values for cylindrical springs bent into a semicircular configuration, providing essential design data for spring-rotor mills. Their work demonstrated that properly designed spring elements exhibit sufficient durability and workability for grinding applications, even under severe cyclic loading conditions.

Ganbat and Gavryushin [10] studied the static and dynamic characteristics of helical spring mills, establishing relationships between spring stiffness, system natural frequencies, and mill operating conditions. They identified operating regimes that minimize undesirable vibrations while maximizing energy transfer to the material being ground.

More recently, Ivannikov et al. [12] conducted comprehensive numerical studies of rotating curved spring dynamics, employing advanced computational methods to simulate the complex interactions between spring elements, material particles, and the grinding

chamber walls. Their results provided valuable insights into the mechanisms of energy dissipation and material comminution within spring-rotor systems.

1.3.3. International Research on Spring Dynamics

Research on spring dynamics extends beyond the specific context of grinding mills, with important contributions from the international community. Lee [6] applied pseudospectral methods to analyze free vibrations of cylindrical helical springs, contributing to the understanding of spring dynamics relevant to mill design. Yildirim [7] investigated linearized disturbance dynamic equations for buckling and free vibration of helical coil springs under combined compression and torsion, providing theoretical foundations for spring element design. Yu and Hao [8,9] developed improved Riccati transfer matrix methods for vibration analysis of non-cylindrical helical springs, extending the analytical capabilities for complex spring geometries.

1.3.4. Alternative Spring-Based Grinding Concepts

Sevostyanov and colleagues [11] developed and investigated needle-milling grinders, representing an alternative approach to spring-based comminution. Their work established scientific foundations for multipurpose needle-milling devices, demonstrating the potential of combined impact-abrasive actions for processing a wide range of materials, including minerals, polymers, and biomass. Comparative studies showed that needle-milling grinders offer advantages in terms of energy efficiency and product uniformity for specific applications [11].

1.3.5. Limitations of Existing Research

Despite these significant contributions, a critical analysis of the literature reveals several important limitations:

1. Predominantly qualitative focus: Most existing studies emphasize mechanical behavior, qualitative performance assessment, and phenomenological observations rather than quantitative optimization [4,5,7,10].
2. Single-factor experimentation: Where quantitative studies exist, they typically employ one-factor-at-a-time approaches that cannot capture interactions between parameters [11,12].
3. Lack of systematic optimization frameworks: No comprehensive methodology has been developed for multi-objective optimization of spring-rotor mills that simultaneously considers throughput, product quality, energy consumption, and wear characteristics [8–13].
4. Limited experimental validation of optimal regimes: Proposed optimal operating conditions are rarely verified through systematic experimental programs [5,12].
5. Absence of robustness analysis: The stability of optimal solutions under realistic industrial variations in feed material properties and operating conditions remains unexplored [9–11].

1.4. Classical and Modern Comminution Theories

Understanding the theoretical foundations of comminution is essential for developing rational optimization approaches. Classical comminution theories provide fundamental relationships between energy consumption and the degree of size reduction, while modern approaches incorporate statistical, thermodynamic, and fracture mechanics concepts.

1.4.1. Classical Theories: Rittinger, Kick, and Bond

Rittinger's theory (1867) states that the energy required for grinding is directly proportional to the new surface area created during comminution [1]:

$$E = A_u \cdot S \tag{1}$$

where A_u is the specific work for new surface formation (kWh/t) and Delta S is the newly created surface area (m^2/kg). This theory is most applicable to fine grinding where surface energy dominates.

Kick's theory (1885) proposes that energy is proportional to the volume or mass reduction of particles [1]:

$$E = k \cdot \ln\left(\frac{D_i}{D_f}\right) \tag{2}$$

where k is a material constant, D_i is initial particle size, and D_f is final particle size. This approach is more suitable for coarse crushing where volume deformation dominates.

Bond's third theory (1952) offers an intermediate relationship, suggesting that work input is proportional to the length of cracks formed [2,3]:

$$E = 10W_i\left(\frac{1}{\sqrt{P_{80}}} - \frac{1}{\sqrt{F_{80}}}\right) \tag{3}$$

where W_i is the Bond work index, P_{80} is the 80% passing size of the product, and F_{80} is the 80% passing size of the feed. Bond's theory has become an industry standard for preliminary mill sizing and energy estimation [2,3].

1.4.2. Limitations of Classical Theories

Despite their widespread use, classical comminution theories have significant limitations when applied to modern fine grinding equipment:

1. They do not account for equipment-specific design features: Parameters such as rotor overlap, chamber clearance, and spring element dynamics in spring-rotor mills have no representation in classical theories [4–6].
2. They fail to capture parameter interactions: Classical theories treat comminution as a single-parameter process, ignoring the complex interactions between multiple operating variables [8–10].
3. They cannot address multi-objective optimization: These theories provide only energy-size relationships, offering no guidance for balancing conflicting objectives such as throughput, product quality, and energy consumption [11–13].
4. They assume material homogeneity: Real feed materials exhibit significant variability in mechanical properties, which classical theories cannot accommodate [14–16].
5. They are empirically derived with limited mechanistic basis: The empirical constants in these theories lack clear physical interpretation and must be determined experimentally for each material–equipment combination [17,18].

1.4.3. Modern Theoretical Developments

Modern theoretical approaches extend classical theories by considering the energy components associated with elastic and plastic deformations [14,15]:

$$A = \left(A_{upr} + A_{pl}\right) + A_s \tag{4}$$

where A_{upr} and A_{pl} represent energies consumed in elastic and plastic deformations, and A_s is the energy required for new surface formation. This approach recognizes that comminution efficiency depends on the proportion of input energy actually used for surface creation.

Doudkin and colleagues have contributed to the understanding of deformation processes in related mechanical systems [14–18]. Their work on mathematical modeling of deformations in steel rolls [14], force determination in milling-rotary equipment [15], and development of vibroscreen feed elements [16] provides valuable methodological foundations applicable to grinding process optimization. Studies on strengthening of low-carbon alloy steel [17] and impact-rotor working equipment [18] further contribute to the understanding of material behavior under dynamic loading conditions relevant to spring-rotor mills.

Research on soil cutting and fracture mechanics [19–25] offers additional insights into material fragmentation processes. Studies on brittle fracture conditions [21], soil–tool interaction modeling [22], numerical methods for soil cutting [23], discrete and continuum modeling [24], and mechanical properties of engaging surfaces [25] provide methodological approaches applicable to modeling comminution processes.

1.5. Optimization Approaches in Grinding Processes

1.5.1. Statistical Design of Experiments (DOE) and Response Surface Methodology (RSM)

Recent years have seen increasing application of statistical optimization methods to grinding processes. Design of Experiments (DOE) enables systematic investigation of multiple factors with minimal experimental effort while capturing interactions between variables [26–29]. Response Surface Methodology (RSM) extends DOE by fitting second-order polynomial models that describe the relationship between input factors and output responses, enabling prediction and optimization within the experimental domain [30–32].

Trivan and Kostić [27] applied multiple linear regression to evaluate excavator energy consumption and cutting resistance, demonstrating the effectiveness of statistical approaches for mining equipment optimization. Qiang et al. [28] developed energy-saving control strategies for bulldozers based on fuel consumption minimization, employing regression techniques to model equipment performance. Klanfar et al. [29] conducted calculation analysis of bulldozer productivity, further demonstrating the utility of statistical methods for earth-moving equipment optimization.

In the context of grinding, Kumar et al. [31] comprehensively reviewed energy-efficient ultrafine grinding in stirred mills, highlighting the potential of RSM for process optimization. Their analysis showed that properly designed statistical experiments can reduce energy consumption by 15–25% compared to conventional operating practices.

1.5.2. Multi-Objective Optimization Methods

The inherent conflict between grinding performance objectives—maximizing throughput and product quality while minimizing energy consumption and equipment wear—necessitates multi-objective optimization approaches.

Pareto optimization provides a framework for identifying non-dominated solutions where no objective can be improved without degrading another [30,32]. The Pareto front visualizes the trade-off surface, enabling decision-makers to select operating points aligned with production priorities.

Evolutionary algorithms, particularly NSGA-II (Non-dominated Sorting Genetic Algorithm II), have proven highly effective for multi-objective optimization in engineering applications [30,32]. NSGA-II employs elitist crowding distance assignment and non-dominated sorting mechanisms to generate diverse sets of Pareto-optimal solutions in a single optimization run.

Li et al. [30] successfully applied NSGA-II to optimize process parameters for robotic grinding, demonstrating the algorithm's ability to handle complex nonlinear relationships between multiple objectives. Their work achieved simultaneous improvements in surface quality and material removal rate.

Wang et al. [32] combined population balance models with RSM for industrial grinding circuit optimization, showing that integrated modeling approaches can capture both micro-scale particle dynamics and macro-scale process behavior. Marijnissen et al. [33] simulated the comminution process in high-speed rotor mills based on feed material properties, providing additional validation for modeling approaches.

1.5.3. Applications to Specific Mill Types

Ball mill optimization has received extensive attention, with studies focusing on media size distribution, mill speed, filling ratio, and liner design [27–29]. However, these models require extensive parameter estimation and are specific to ball mill geometry.

Stirred mill optimization studies have emphasized media size, stirrer speed, and slurry properties, demonstrating significant energy savings compared to ball mills for fine grinding applications [31].

1.5.4. Research Gap Specific to Spring-Rotor Mills

Despite the extensive literature on grinding optimization, a critical analysis reveals a substantial gap: no comprehensive multi-objective optimization framework exists specifically for spring-rotor mills. The unique design features of these devices—rotor overlap, chamber clearance, and spring element dynamics—have not been systematically incorporated into optimization studies. Previous research on spring-rotor mills has established mechanical feasibility and qualitative performance characteristics [4–7,10–13], but quantitative optimization with experimental validation remains absent from the literature.

Furthermore, existing studies have not addressed the robustness of optimal solutions under realistic industrial variations in feed material properties and operating conditions. The stability of optimized regimes to parameter fluctuations is essential for practical implementation but has received little attention.

1.6. Research Objectives and Scientific Novelty

1.6.1. Problem Statement

Consequently, there exists a scientifically and practically significant problem: current approaches to optimizing spring-rotor mills are predominantly based on single-criterion empirical tuning or simplified models that fail to capture the complex nonlinear interactions between key technological parameters. While classical comminution theories provide a foundation, they do not account for the specific design features of spring-rotor equipment, such as rotor overlap and chamber clearance, nor do they offer a systematic framework for multi-objective optimization where throughput, product quality, and energy consumption must be considered concurrently [8–13]. Previous studies on spring-rotor mills have established mechanical feasibility and qualitative performance characteristics [4–7,10–13], but systematic quantitative optimization with experimental validation remains absent from the literature.

1.6.2. Research Objectives

The primary objectives of this study are:

1. To develop a comprehensive experimental database for spring-rotor mill performance through a five-factor Hartley experimental design, systematically varying rotational speed, filling ratio, rotor overlap, chamber clearance, and grinding time.

2. To construct adequate second-order polynomial regression models ($R^2 > 0.93$) describing the influence of these factors on five key performance indicators: grinding fineness, throughput, power consumption, specific energy consumption, and specific metal intensity.
3. To apply multi-objective optimization methods, including Pareto front analysis and weighted sum aggregation, to identify compromise optimal operating regimes that balance conflicting performance requirements.
4. To experimentally verify the predicted optimal regimes through independent confirmatory experiments and assess solution robustness through Monte Carlo simulation.
5. To develop practical recommendations for industrial implementation, including permissible parameter variation ranges and expected performance improvements.

1.6.3. Scientific Novelty

The scientific novelty of this work lies in the following:

1. First comprehensive RSM application to spring-rotor mills: for the first time, a complete second-order response surface methodology is applied to a spring-rotor mill, quantitatively describing the influence of five key factors on five performance indicators. This extends beyond qualitative assessments and single-factor studies prevalent in previous research [4–7,10–13].
2. Novel multi-objective optimization framework incorporating equipment-specific parameters: a novel application of the NSGA-II evolutionary algorithm to visualize the Pareto-optimal front in the space of conflicting criteria (fineness, throughput, power) is presented, explicitly incorporating design-specific parameters unique to spring-rotor mills (rotor overlap and chamber clearance). This provides a clear tool for engineering decision-making that has not previously been available for this equipment class [30,32].
3. First quantification of parameter interactions for spring-rotor mills: the study quantifies, for the first time, the interaction effects between key operating parameters, revealing previously unknown synergistic and antagonistic relationships that significantly impact process performance.
4. Experimentally verified optimal regimes with robustness analysis: the study provides experimentally verified, robust optimal operating regimes that yield quantifiable improvements (15–20% higher throughput, 8–12% lower energy consumption) compared with traditional empirical tuning methods. The inclusion of Monte Carlo robustness analysis represents a methodological advance over studies that identify optimal points without assessing their stability [27–29].
5. Integrated framework from design to implementation: the research presents an integrated framework spanning experimental design, mathematical modeling, multi-objective optimization, experimental verification, and practical implementation guidelines—a comprehensive approach not previously applied to spring-rotor mills.

1.6.4. Practical Significance

The practical significance of this research extends beyond academic contributions. The developed methodology and specific optimal operating regimes can be directly implemented in industrial settings to:

- increase mill throughput by 15–20% without additional capital investment;
- reduce specific energy consumption by 8–12%, contributing to sustainability goals;
- decrease production costs by approximately 10% through combined efficiency improvements;
- provide operators with clear, quantitative guidelines for process tuning;

– enable informed decision-making based on production priorities (quality, throughput, or energy efficiency).

Furthermore, the methodological framework is transferable to other types of grinding equipment and similar multi-parameter processes in mineral processing, chemical engineering, and materials manufacturing.

1.7. Paper Organization

The remainder of this paper is organized as follows. Section 2 describes the experimental setup, materials, design of experiments, regression modeling methodology, and multi-objective optimization approach in detail. Section 3 presents experimental results, regression models, statistical validation, and comprehensive analysis of factor effects on process throughput, including linear, quadratic, and interaction effects. Section 4 discusses multi-objective optimization outcomes, including Pareto front visualization, identification of compromise optimal regimes, verification experiments, robustness analysis, and industrial implications. Section 5 provides conclusions, summarizes key contributions, and offers practical recommendations for industrial implementation.

2. Materials and Methods

2.1. Study Object and Experimental Setup

The object of the study was the technological process of grinding bulk mineral materials in a laboratory-scale spring-rotor mill of an original design (Figure 2). The apparatus consists of a sealed housing equipped with feed and discharge ports, inside which two counter-rotating spring-rotor disks are mounted on a common shaft [17]. Working elements in the form of cylindrical helical springs made of 65 G spring steel are fixed at the periphery of the disks. Their rotation inside the housing provides a combined impact-abrasive loading of the processed material.

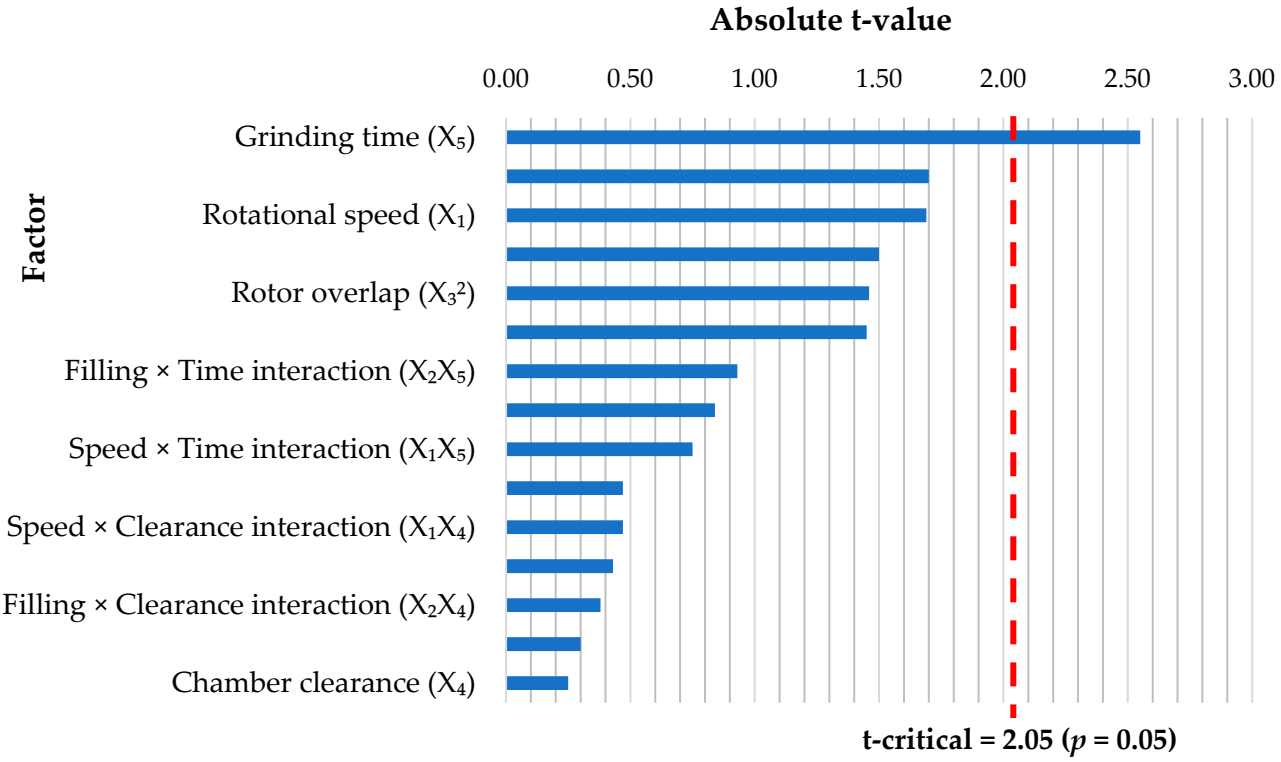


Figure 2. Pareto chart of standardized effects for throughput (P).

The design allows continuous adjustment of the key geometric parameters, including the overlap (engagement) of the working zones of the counter-rotating rotors (X_3) and the axial clearance between the rotors and the chamber wall (X_4). To enable a quasi-continuous operating mode and in situ product classification during grinding, an inter-section bypass diaphragm with calibrated through-holes can be installed [18–21].

The mill design provides for rapid adjustment of the key geometric parameters that directly affect the kinematics and hydrodynamics of the grinding process [22]:

- the rotor overlap (X_3) is adjusted by axial displacement of one rotor disk relative to the other using calibrated spacers. The adjustment range is from −15 mm (separation) to +15 mm (overlap);
- the axial clearance (X_4) is regulated by varying the distance between the spring ends and the side wall of the grinding chamber;
- a replaceable diaphragm (mesh-type or slotted) can be installed in the inter-rotor space to enable quasi-continuous operation and preliminary in-process classification of the product during grinding.

The electromechanical subsystem includes a 15 kW induction motor (item 6) (manufactured by UNIPUMP, Russia) connected via a variable-frequency drive (VFD) manufactured by VEDA MC (Russia). The use of the VFD enables soft starting, stepless control of the rotational speed in the range of 0–3000 rpm, and stabilization of the preset speed under varying load conditions [23,24].

Main technical specifications of the experimental setup:

- grinding chamber volume: 5.0 L;
- rated power of the drive induction motor: 15.0 kW;
- control system: variable-frequency drive with precise speed setting and stabilization;
- monitoring and measurement system: digital wattmeter (±0.5% accuracy) for power consumption measurement, optical tachometer sensor (±1 rpm accuracy), and electronic scales for dosing (±1 g accuracy) [25].

2.1.1. Feed Materials Characterization

Preliminary single-factor experiments were conducted using two types of mineral materials to assess their grinding behavior, limestone and marble chips, both with an initial particle size fraction of 5–7 mm. The physical and mechanical properties of these materials are summarized in Table 1.

Table 1. Physical and mechanical properties of feed materials.

Parameter	Limestone	Marble Chips
Particle size fraction, mm	5–7	5–7
Uniaxial compressive strength σ_c, MPa	80	110
Young's modulus E, MPa	35×10^3	55×10^3
Bulk density ρ, t/m^3	2.4	2.6
Hardness (Mohs scale)	3	3–4
Brittleness	High	Medium

After a series of single-factor experiments, marble chips were selected as the primary feed material for the subsequent multifactor experimental design and regression modeling. This decision was based on the material's higher strength characteristics and more consistent fracture behavior, which provides a more rigorous test of the grinding process and ensures that the resulting optimization framework is applicable to a wider range of materials with medium to high hardness. Marble chips are a brittle but durable natural

material consisting predominantly of calcite. Despite its brittleness, which facilitates initial fracture, the material exhibits good resistance to wear and consistent behavior under repeated impact-abrasive loading. All subsequent multifactor experimental results presented in this study were obtained using marble chips as the feed material.

2.1.2. Particle Size Analysis Method

Grinding fineness, denoted as R_{-71} (%), is defined as the mass percentage of the ground product passing through a 71 μm sieve. The choice of 71 μm as the critical particle size threshold is based on several considerations:

1. Regulatory compliance: According to relevant standards [26], the 71 μm sieve is designated as a "control sieve" for fine mineral powders. Material is considered compliant if the residue on this sieve does not exceed a specified percentage, making it a standard benchmark for fineness assessment.
2. Industrial relevance: The 71 μm sieve is widely used in particle size analysis for various materials, including cement fineness determination, mineral powder classification, quality control of quartz sand, ore processing, food powders, and pharmaceutical applications where the absence of particles larger than 71 μm is critical for product quality [27–29].
3. Material-specific application: For marble chips, the 71 μm sieve serves as a boundary for determining the content of dust-like and clay particles, providing a reliable indicator of product purity and grinding efficiency.

Particle size distribution was determined by sieve analysis using a standardized method. After each grinding cycle, the entire product mass was subjected to sieving through a nested set of sieves, with the 71 μm sieve as the control mesh. The fraction retained on each sieve was weighed using electronic scales (±1 g accuracy), and the percentage passing the 71 μm sieve was calculated as:

$$R_{-71} = \frac{m_{pass}}{m_{total}} \times 100\% \quad (5)$$

where m_{pass} is the mass of material passing the 71 μm sieve, and m_{total} is the total mass of the ground product. Each measurement was performed in triplicate, and the average value was used for subsequent analysis. The coefficient of variation for repeated measurements did not exceed 6%, confirming good reproducibility of the sieving method.

2.2. Design of Experiments and Response Variables

To minimize the number of experimental runs while preserving data representativeness, a five-factor rotatable second-order composite design (Hartley plan) was employed. This design is optimal for constructing second-order polynomial response surface models, as it ensures uniform prediction variance in all directions from the design center and enables reliable estimation of quadratic effects [27–29]. The Hartley design provides sufficient information on the influence of multiple factors on the process outcomes while keeping the experimental effort at a minimum [30].

The total number of experimental runs was $N = 2^{(k-1)} + 2k + n_0 = 16 + 10 + 3 = 27$, where k—the number of factors ($k = 5$); n_0—the number of center-point runs used to estimate the pure error and to assess model adequacy ($n_0 = 3$).

The sequence of all 27 experimental runs was fully randomized to eliminate the influence of systematic drifts (e.g., temperature variations, equipment wear, and operator-related effects).

The independent variables (in both coded and natural units) were defined as follows:

- X_1—rotational speed of the working elements, n (rpm);

- X_2—degree of filling of the grinding chamber with material, k_m (dimensionless);
- X_3—overlap (engagement) of the working zones of the driving and driven rotors, k_r (mm); negative values correspond to rotor separation;
- X_4—clearance between the moving and stationary parts of the grinding chamber, k_{zaz} (mm);
- X_5—grinding cycle duration, T(s).

The factor levels are summarized in Table 2.

Table 2. Factors and levels of variation.

No.	Investigated Factors	Designations	Levels of Variation			Variation Interval
			−1	0	+1	
1	Rotational speed of the working elements, n	X_1	1500	2000	2500	500
2	Material filling ratio, k_m	X_2	0.1	0.3	0.5	0.2
3	Overlap of the working zones of the driving and driven rotors, k_r, mm	X_3	−15	0	+15	15
4	Clearance between the moving and stationary parts of the grinding chamber, k_{zaz}, mm	X_4	2	7	12	5
5	Grinding duration, T, s	X_5	60	90	120	30

After completion of each grinding cycle, the product was subjected to sieve analysis.

As responses to the action of the factors determining the grinding process behavior and for a comprehensive assessment of its efficiency, five output parameters were selected: Y_1—Grinding fineness (R_{-71}), %—content of the fraction with a particle size of less than 71 µm; Y_2—Throughput (P), kg/h—mass of ground material per unit time; Y_3—Drive power (N), kW—consumed electrical power; Y_4—Specific energy consumption (E_{ud}), kWh/t—energy consumption per unit of product; Y_5—Specific metal intensity (M_{ud}), t·h/t—an indirect indicator of equipment wear. All the listed functions meet the requirements imposed on optimization parameters: universality, the possibility of being expressed by a single term, and quantitative representation.

2.3. Mathematical Modeling and Statistical Analysis

The processing of experimental data and the construction of mathematical models were carried out within the framework of the Response Surface Methodology (RSM). It was assumed that the dependence of each response Y on the factors X can be approximated by a second-order polynomial [31]:

$$Y = b_0 + \sum_{i=1}^{5} b_i \cdot X_i + \sum_{i=1}^{5} b_{ii} \cdot X_i^2 + \sum_{i=1}^{4} \sum_{j=i+1}^{5} b_{ij} \cdot X_i \cdot X_j + \varepsilon \quad (6)$$

where Y—calculated value of the response function;

b_0—intercept (coefficient);

b_i—coefficients of linear effects;

b_{ii}—coefficients of quadratic effects;

b_{ij}—coefficients of interaction effects;

X_i—coded values of the factors;

ε—random error.

The processing of experimental data and the construction of mathematical models were carried out within the framework of the Response Surface Methodology (RSM). It

was assumed that the dependence of each response Y on the factors X can be approximated by a second-order polynomial [30] (Equation (6)).

The regression coefficients β (b_0, b_i, b_{ii}, b_{ij}) were estimated using the ordinary least squares (OLS) method. All calculations were performed using specialized statistical analysis software: STATISTICA 10.0 (StatSoft, Tulsa, OK, USA) and Design-Expert 13 (Stat-Ease, Minneapolis, MN, USA).

The statistical significance of each coefficient was tested using Student's t-test. The null hypothesis (that the coefficient equals zero) was rejected at a significance level of $p < 0.05$, indicating that the factor has a statistically significant influence on the response.

The overall adequacy of the model was tested using Fisher's F-test. This involved comparing the residual variance (variation not explained by the model) with the pure reproducibility variance estimated from the three center-point runs (runs No. 17, 18, 27). A lack-of-fit test was also performed; a p-value for lack-of-fit greater than 0.05 indicates that the model fits the data well and there is no significant systematic error.

The quality of approximation of the experimental data was characterized by the coefficient of determination R^2 and the adjusted coefficient of determination R^2adj, which accounts for the number of predictors in the model.

2.4. Multi-Objective Optimization Methodology

Since the objectives associated with improving individual responses are conflicting (for example, increasing grinding fineness leads to a decrease in throughput and an increase in energy consumption), the process tuning problem is multi-objective.

To solve this problem, a combined approach was applied.

Construction of the Pareto-optimal front. For the three most significant criteria (R_{-71}, P, N), the evolutionary algorithm NSGA-II (Non-dominated Sorting Genetic Algorithm II) was employed.

The NSGA-II was selected due to its proven efficiency in handling multi-objective optimization problems with non-linear relationships and multiple conflicting criteria [30,32]. Unlike classical gradient-based methods, NSGA-II does not require differentiability of the objective functions and is capable of generating a diverse set of non-dominated solutions in a single optimization run through its elitist crowding distance assignment and non-dominated sorting mechanisms. This makes it particularly suitable for engineering applications where the goal is to visualize the entire trade-off surface between competing objectives such as product quality, throughput, and energy consumption.

As a result, a set of non-dominated solutions representing the Pareto front in the three-dimensional criterion space was generated. This made it possible to visualize objective technological trade-offs. Aggregation of criteria using the weighted sum method (Weighted Sum Method). To obtain a single compromise solution suitable for practical implementation, the individual criteria were aggregated into a single composite criterion. Prior to aggregation, all responses were normalized to the range [0, 1] with respect to their extreme values within the experimental domain. The integral criterion F(X) was formulated as a weighted sum:

$$F(X) = \omega_1 \cdot f_1(X) + \omega_2 \cdot f_2(X) + \omega_3 \cdot f_3(X) + \omega_4 \cdot f_4(X) + \omega_5 \cdot f_5(X) \rightarrow min, \quad (7)$$

where f_1(X)—normalized value of the i-th response; ω_1—weighting coefficients reflecting technological priorities: ω_1 = 0.30 (grinding fineness), ω_2 = 0.25 (throughput), ω_3 = 0.20 (power), ω_4 = 0.15 (specific energy consumption), and ω_5 = 0.10 (specific metal intensity). The sum of ω_r = 1.

The selection of these weighting coefficients was based on the typical priorities of industrial grinding processes, established through expert consultation and analysis of com-

mon practice in mineral processing and waste recycling applications. In these industries, product quality, represented here by grinding fineness (R_{-71}), is typically the primary constraint that must be satisfied first; hence, it receives the highest weight (ω_1 = 0.30). Throughput (P) is the main driver of process efficiency and economic return, justifying the second-highest weight (ω_2 = 0.25). Power consumption (N) represents a direct operating cost, while specific energy consumption (E_{ud}) reflects the overall energy efficiency of the process; together they account for a combined weight of 0.35, emphasizing the importance of energy savings. Finally, specific metal intensity (M_{ud}), an indicator of equipment wear and maintenance costs, receives a lower weight (ω_5 = 0.10) as it is a longer-term operational consideration. The chosen weights reflect a balanced, practical approach to process optimization.

2.5. Stability Analysis and Verification

The robustness of the identified optimum with respect to small random variations in the input parameters was examined using the Monte Carlo method (N = 10,000 iterations). The final optimal solution was verified through three confirmatory experiments.

All calculations, statistical analysis, plotting, and numerical optimization were performed using specialized software packages: STATISTICA 12.0 (StatSoft, Tulsa, OK, USA), Design-Expert® 13 (Stat-Ease, Minneapolis, MN, USA), and the MATLAB R2021a environment (MathWorks, Natick, MA, USA) with built-in optimization tools.

3. Results and Discussion

3.1. Experimental Data and Preliminary Analysis

The complete experimental design matrix (27 runs) with the averaged values of the response variables obtained from three parallel measurements is presented in Table 2. Already at this stage, visual inspection of the data makes it possible to identify a number of patterns. For example, experiments with the maximum rotational speed (X_1 = +1) and minimum grinding time (X_5 = −1) generally demonstrate high throughput (P up to 23.3 kg/h, run No. 7), while the grinding quality deteriorates (R_{-71} = 24.2%). In contrast, prolonged grinding (X_5 = +1), even at a moderate rotational speed, promotes the production of a finer product (R_{-71} = 10.4%, run No. 14). The drive power consistently increases with increasing rotational speed and chamber filling ratio.

The results of the three center-point runs (No. 17, 18, 27) were used to estimate the reproducibility variance (S^2_{vospr}). The calculated coefficient of variation for the main responses (P, R_{-71}) did not exceed 6%, which is significantly lower than the accepted allowable level of 13%, confirming good experimental reproducibility.

3.2. Regression Models and Adequacy Assessment

Based on the data in Table 2, regression equations in coded variables for all five response functions were obtained using the least squares method. After testing the significance of the coefficients using Student's t-test ($p < 0.05$), insignificant terms were excluded, and the models took the following form (key statistically significant coefficients are presented):

- for grinding fineness

$$R_{-71} = 12.1 + 0.04n + 8.4{\cdot}10^2{\cdot}k_m - 5{\cdot}10^2{\cdot}k_p + 0.65T - 1.4{\cdot}10^3{\cdot}k_m^2 - 8.8{\cdot}10^2{\cdot}k_p - 0.85k_{zaz}^2; \quad (8)$$

- for throughput:

$$P = 8.6 - 5 \cdot 10^{-4} \cdot n + 5.62 \cdot 10^{2} k_m + 6 \cdot 10^{2} \cdot k_p + 1.4 \cdot k_{zaz} + 0.01T - \\ -4 \cdot 10^{3} \cdot k_m^2 - 3.65 \cdot 10^{3} \cdot k_p^2 - 0.45 k_{zaz}^2 + \\ +2 \cdot 10^{-3} T^2 + 3 \cdot 10^{-3} n \cdot k_{zaz}; \quad (9)$$

- for drive power:

$$N = 26.3 - 4 \cdot 10^{-3} n - 7.6 \cdot k_p - 13.3 \cdot k_m - 1.4 \cdot k_{zaz} + 0.13T + \\ +2 \cdot 10^{-6} n^2 + 23.6 \cdot k_m^2 - 0.16 \cdot k_{zaz}^2 + 0.01 n \cdot k_m - 0.31 \cdot k_m \cdot T; \quad (10)$$

- for specific energy consumption:

$$E_{ud} = 5.1 + 3 \cdot 10^{-3} n + 10.1 \cdot k_m - 1.12 \cdot k_p + 1.4 \cdot k_{zaz} - 0.3T - \\ -0.1 \cdot 10^{-6} n^2 - 2.6 k_m^2 - 1.6 \cdot 10 \cdot k_p^2 - 0.15 k_{zaz}^2 - 2 \cdot 10^{-3} T^2; \quad (11)$$

- for specific metal intensity:

$$M_{ud} = 0.21 - 3 \cdot 10^{-4} n + 16.5 k_p + 0.27 k_{zaz} + \\ +0.02T - 6.2 k_p^2 - 2 \cdot 10^{-2} k_{zaz}^2. \quad (12)$$

The dimensionality of the studied parameters presented in natural units is as follows: rotational speed—rpm; grinding duration—s; clearance and overlap—mm; material filling ratio—dimensionless.

The statistical characteristics of the obtained models are summarized in Table 3. High values of the coefficients of determination ($R^2 > 0.93$ for all models) and adjusted coefficients of determination ($R^2_{adj} > 0.91$) indicate that the models explain more than 93% of the variance of the experimental data.

Table 3. Experimental design matrix and averaged values of the response functions.

No.	X_0	X_1	X_2	X_3	X_4	X_5	Experimental Results				
							R_{-71}, %	$N \cdot 10^{-1}$, kW	E_{ud}, (kWh)/t	P, kg/h	M_{ud}, T·h/t
1	1	1	1	1	1	1	12.0	7.3	9.3	7.9	0.63
2	1	−1	−1	1	1	1	14.2	1.7	5.3	3.2	1.56
3	1	−1	1	−1	−1	−1	38.0	2.1	2.1	10.0	0.5
4	1	1	−1	−1	−1	−1	28.0	4.5	2.9	15.0	0.3
5	1	−1	1	−1	1	1	26.3	2.0	5.3	3.8	1.32
6	1	1	−1	−1	1	1	16.8	3.3	6.1	5.4	0.9
7	1	1	1	1	−1	−1	24.2	14.2	6.2	23.3	0.2
8	1	−1	−1	1	−1	−1	26.2	1.7	2.1	8.2	0.6
9	1	−1	1	1	1	−1	28.1	5.1	4.3	11.9	0.42
10	1	1	−1	1	1	−1	18.0	9.1	5.1	6.8	0.27
11	1	1	1	−1	−1	1	22.0	4.8	7.1	2.1	0.7
12	1	−1	−1	−1	−1	1	24.3	1.0	3.1	2.1	2.4
13	1	−1	1	1	−1	1	20.0	2.2	6.3	3.4	1.41
14	1	1	−1	1	−1	1	10.4	4.1	7.3	5.5	0.9
15	1	1	1	−1	1	−1	30.1	11.1	5.1	21.8	0.23
16	1	−1	−1	−1	−1	−1	32.0	0.8	1.1	7.8	0.64
17	1	0	0	0	0	0	29.0	3.7	5.0	7.4	0.67

Table 3. *Cont.*

No.	X_0	X_1	X_2	X_3	X_4	X_5	Experimental Results				
							R_{-71}, %	$N \cdot 10^{-1}$, kW	E_{ud}, (kWh)/t	P, kg/h	M_{ud}, T·h/t
18	1	0	0	0	0	0	20.1	5.9	5.2	9.8	0.51
19	1	1	0	0	0	0	26.0	1.7	3.7	4.8	1.04
20	1	−1	0	0	0	0	25.1	4.9	5.8	8.5	0.58
21	1	0	1	0	0	0	21.9	2.6	4.2	6.3	0.79
22	1	0	−1	0	0	0	19.8	4.5	5.8	7.0	0.63
23	1	0	0	1	0	0	27.3	2.9	4.3	7.0	0.71
24	1	0	0	−1	1	0	22.5	4.0	5.3	7.6	0.65
25	1	0	0	0	−1	0	24.9	3.4	3.7	7.4	0.67
26	1	0	0	0	0	1	18.0	3.1	6.3	4.9	1.01
27	1	0	0	0	0	−1	28.3	5.4	3.7	14.8	0.33

The results of the analysis of variance (ANOVA) confirm the overall statistical significance of the regression models (p-value for the F-test < 0.001). Moreover, the ratio of the calculated F-value to the tabulated F-value for all models exceeds 10, and the p-value for the lack of fit > 0.05, which indicates the adequacy of the developed models and the absence of systematic error (Table 4).

Table 4. Statistical characteristics of regression model adequacy.

Model	Coefficient of Determination R^2	Adjusted R^2	Standard Error	F-Test	p-Value
R_{-71}	0.954	0.942	0.87	79.3	<0.001
P	0.962	0.951	0.42	88.7	<0.001
N	0.947	0.933	0.38	72.5	<0.001
E_{ud}	0.938	0.921	0.35	65.8	<0.001
M_{ud}	0.931	0.912	0.09	59.4	<0.001

Based on the obtained regression equations, three-dimensional response surfaces can be readily constructed to visualize the process behavior. However, to quantitatively assess the contribution of each factor and prioritize them for process control, a Pareto chart of the standardized effects was constructed for the key response of throughput (P) (Figure 3). This chart ranks the absolute values of the t-statistics for each model term; bars extending beyond the red reference line (representing the critical t-value at $p = 0.05$) indicate statistically significant effects.

The analysis of Figure 2 confirms that grinding time (X_5) and rotational speed (X_1) are the most influential factors, exhibiting the largest linear effects. The high significance of the quadratic terms for speed (X_1^2) and filling ratio (X_2^2) confirms the nonlinear nature of the process and the existence of well-defined optima. Notably, the interaction between speed and time (X_1X_5) is also significant, indicating that these two parameters must be optimized jointly. Factors such as the linear effect of clearance (X_4) show a relatively weak influence on throughput, suggesting that this parameter can be primarily adjusted to optimize other objectives like energy consumption or product fineness.

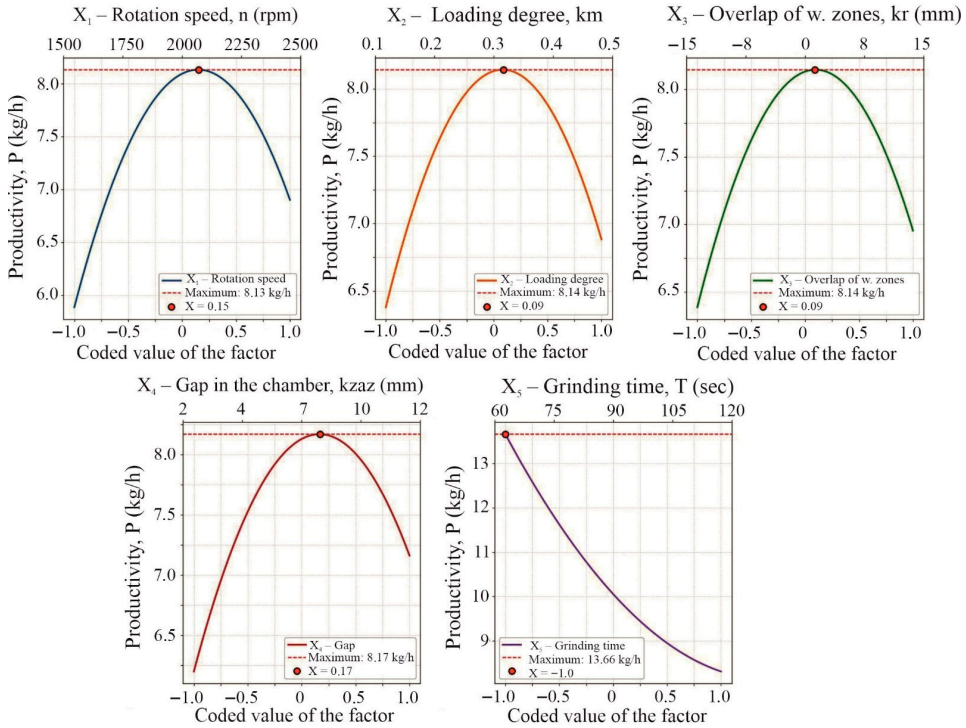


Figure 3. Effect of technological factors on throughput.

A detailed analysis of the influence of all factors on throughput, including their linear, quadratic, and interaction effects, is presented in the following section.

3.3. Analysis of Factor Effects on Process Throughput

Considering the technological importance of throughput (P) as a key performance indicator of the grinder, primary attention was devoted to its analysis. The results of the analysis of variance (ANOVA) for the throughput regression model (4) and the analysis of standardized coefficients made it possible to quantitatively assess the contribution of each factor and to identify optimal regions. The corresponding results are presented as follows: Figure 3 shows the plots of the effects of the main factors on throughput, and Figure 4 presents the analysis of the influence of the main factors on throughput.

(A) Linear effects of factors

The analysis of the coefficients of the linear terms of the throughput model revealed the following ranking of factors according to the strength of their influence (in descending order of absolute coefficient values) [20].

1. X_5 (grinding time): −2.55—the negative sign indicates a decrease in throughput with increasing time; this is the largest linear effect in absolute value. An increase in time by 30 s reduces throughput by 2.55 kg/h.
2. X_1 (rotational speed): +1.69—the positive sign indicates an increase in throughput with increasing speed. Each increase in speed by 500 rpm increases throughput by 1.69 kg/h.
3. X_2 (filling ratio): +0.75—the positive sign indicates that increasing the filling ratio promotes an increase in throughput. However, there exists an optimal value beyond which the effect decreases.
4. X_3 (overlap of working zones): +0.30—a weak positive effect indicating a slight improvement in throughput with increasing overlap.
5. X_4 (chamber clearance): −0.25—a negative but minimal effect. An increase in clearance slightly reduces throughput.

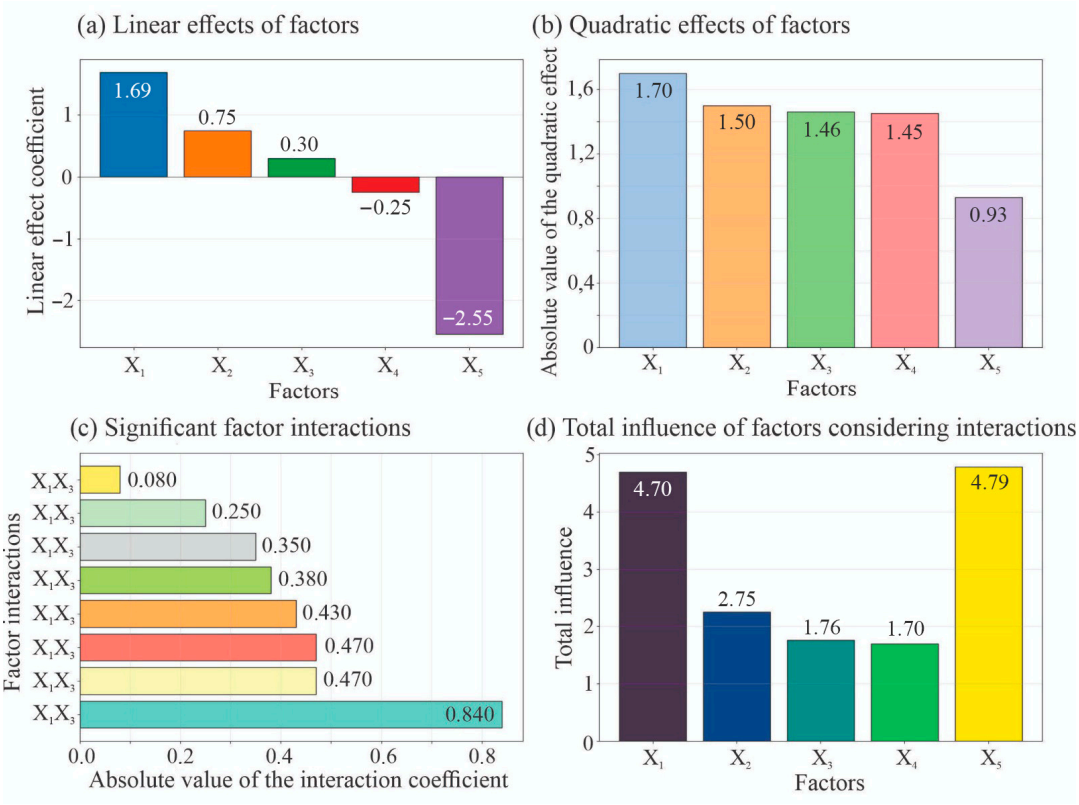


Figure 4. Analysis of the influence of the main factors on throughput.

(B) Quadratic effects of factors

The quadratic effects in the throughput model characterize the nonlinearity of factor influences and the presence of optima within the investigated range. All quadratic-term coefficients (except X_5^2) are negative, indicating a concave response surface with a maximum in the vicinity of the central region of the design.

Ranking of factors according to the magnitude of the quadratic effect (by absolute value):

1. X_1 (rotational speed): −1.70—the highest nonlinearity, with a sharp change in P when deviating from the optimal value (~2074 rpm).
2. X_2 (filling ratio): −1.50—a substantial effect, especially when the chamber is overloaded beyond the optimal level.
3. X_3 (overlap of working zones): −1.46—moderate nonlinearity.
4. X_4 (chamber clearance): −1.45—an influence similar to that of the overlap.
5. X_5 (grinding time): +0.93—the only positive quadratic effect, indicating a convex dependence along this factor.

The negative quadratic coefficients for X_1–X_4 indicate the existence of optimal values of each parameter at which maximum throughput is achieved. Deviations from these optimal values in either direction lead to a decrease in throughput.

The positive quadratic coefficient for X_5 indicates the presence of a minimum throughput within the investigated domain, followed by an increase with further increase in time.

(C) Factor interactions

The analysis of the interaction coefficients in the throughput model revealed a non-additive nature of the influence of the technological parameters, indicating the presence of synergistic and antagonistic effects under their joint variation.

Figures 5 and 6 present visualizations of the combined effects of the factors on throughput.

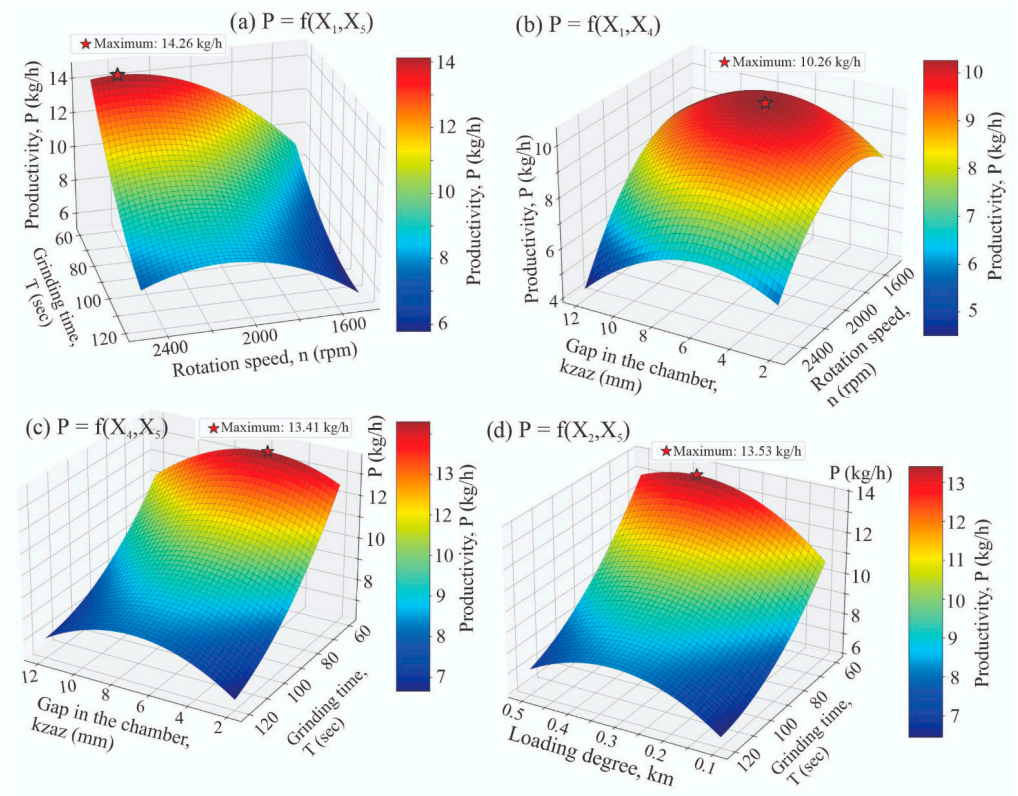


Figure 5. 3D response surfaces of throughput as a function of pairs of key factors.

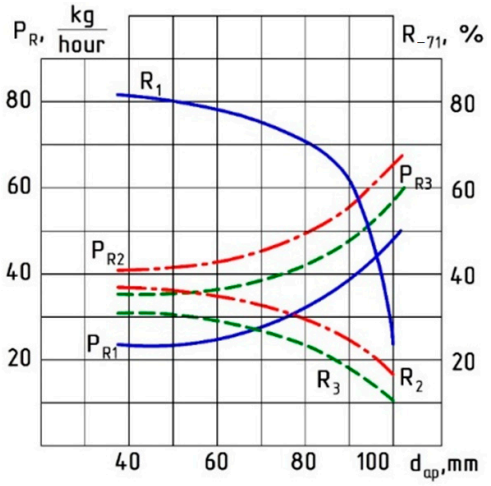


Figure 6. Dependence of throughput P and fineness R_{-71} on the diaphragm orifice diameter d_{dg} at different axial clearances X: (1) X = 2 mm; (2) X = 7 mm; (3) X = 12 mm.

The key interactions and their interpretation are as follows.

1. X_1X_5 (Speed × Time): −0.84—the strongest negative interaction. An increase in grinding time at high rotational speed leads to a more pronounced decrease in throughput.
2. X_1X_4 (Speed × Clearance): +0.47 and X_4X_5 (Clearance × Time): +0.47—positive interactions indicating the possibility of compensating negative effects.
3. X_2X_4 (Filling ratio × Clearance): +0.43—a positive interaction improving throughput under the joint increase in filling ratio and clearance.
4. X_2X_5 (Filling ratio × Time): −0.38—a negative interaction that amplifies the adverse effect of time at high filling ratios.

Technological implications:

- the X_1X_5 interaction indicates the need for joint optimization of speed and time—both parameters should not be set to their maximum values simultaneously;
- the positive interactions X_1X_4 and X_4X_5 make it possible to partially compensate for the negative effects of other factors by adjusting the clearance;
- particular attention should be paid to interactions involving grinding time (X_5) as the most influential factor.

In Figure 6, based on preliminary experiments, the dependences of throughput P and fineness R_{71} on the diaphragm orifice diameter d_{dg} at different axial clearances X are presented.

Analysis of the plot in Figure 6 shows that with increasing diaphragm orifice diameter d_{dg} and axial clearance, the mill throughput increases; however, a decrease in grinding quality is observed.

Figure 7 presents the dependence of grinder throughput on the rotational speed of the working elements at different processing times. The remaining experimental factors (filling ratio, overlap of the working zones, and grinding chamber clearance) are fixed at the mean level (X = 0). The analysis indicates that maximum throughput is achieved at a rotational speed of 2100–2200 rpm and a grinding time of 90–100 s.

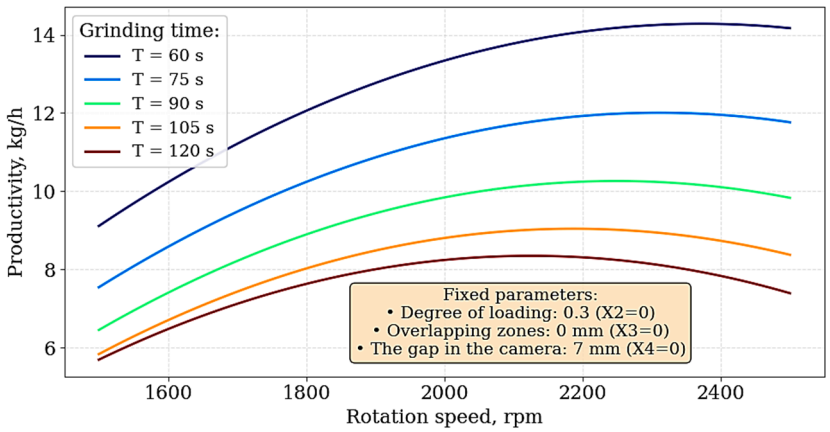


Figure 7. Dependence of throughput on rotational speed at different grinding times.

(D) Physical interpretation of the results

1. The influence of grinding time (X_5) exhibits a linear effect of −2.55, indicating that an increase in time beyond the optimal value (132 s) leads to a decrease in throughput. However, the positive quadratic effect (+0.93) indicates a complex dependence—beyond a certain threshold, throughput begins to increase. Physically, this can be explained by the fact that excessive grinding leads to particle aggregation and increased energy consumption without a substantial improvement in product yield.
2. The influence of rotational speed (X_1) is characterized by a positive linear effect (+1.69) and a strong negative quadratic effect (−1.70), indicating the existence of a well-defined optimum (~2074 rpm). At low speeds, the impact energy is insufficient, whereas at high speeds parasitic effects (aeration, centrifugal forces) arise.
3. The influence of the filling ratio (X_2) exhibits a positive linear effect (+0.75), indicating an increase in throughput with increasing loading, while the quadratic effect (−1.50) limits this increase. The optimum is achieved at a filling ratio of 32.5%.

4. The influence of the overlap of the working zones (X_3) shows a weak positive effect (+0.30) with moderate nonlinearity (−1.46), indicating the presence of an optimal value near zero (0 mm). This corresponds to the neutral position of the rotors.
5. The influence of the chamber clearance (X_4) exhibits a slight negative linear effect (−0.25) with moderate nonlinearity (−1.45). The optimum is located in the center of the design space (7 mm). The clearance has a greater effect on energy consumption than on throughput.
6. These physical interpretations are consistent with the fundamental mechanisms of comminution in spring-rotor mills. The combined impact-abrasive action means that particle breakage occurs through two primary modes: (1) high-velocity impacts between particles and the rotating spring elements, governed by kinetic energy ($\propto n^2$), and (2) inter-particle abrasion in the compressed zone between rotors, governed by residence time and filling ratio. The identified quadratic effects and interactions quantitatively capture the transition between these modes. For instance, the negative interaction X_1X_5 (speed × time) indicates that beyond an optimal point, prolonged exposure to high-intensity impacts leads to diminishing returns, possibly due to particle agglomeration or the ejection of fine particles from the active zone before complete breakage. The positive interaction X_2X_4 (filling ratio × clearance) suggests that a larger clearance allows for better material circulation, accommodating higher fill levels without clogging the rotor–stator gap.

4. Multi-Objective Optimization of Throughput and Technological Performance Indicators

The grinding process is characterized by the need to simultaneously account for a number of conflicting requirements. Thus, increasing grinding fineness (R_{71}) usually requires an increase in processing time and energy consumption, which leads to a decrease in throughput and an increase in specific energy consumption (E_{ud}). Therefore, the process tuning problem is inherently multi-objective and requires the identification of compromise solutions that ensure an acceptable balance among all target performance indicators.

4.1. Formulation of the Multi-Objective Optimization Problem

Based on the developed adequate regression models (Equations (9)–(12)), the problem was formulated as follows:

Objective functions (responses) to be optimized:

1. $Y_1 = R_{71}(X) \rightarrow$ min (maximization of grinding fineness);
2. $Y_2 = P(X) \rightarrow$ max (maximization of throughput);
3. $Y_3 = N(X) \rightarrow$ min (minimization of power consumption);
4. $Y_4 = E_{ud}\ (X) \rightarrow$ min (minimization of specific energy consumption);
5. $Y_5 = M_{ud}\ (X) \rightarrow$ min (minimization of specific metal intensity).

Vector of control factors (in natural units): $X = [n, k_m, k_r, k_{zaz}, T]$. Imposed constraints: the factors vary within the ranges defined by the experimental design (Table 1).

4.2. Visualization of Throughput Optimality Regions

For visual identification of the factor ranges ensuring high throughput, a series of contour plots was constructed. Figure 8 presents the region where the throughput is at least 95% of its maximum predicted value. This region (shaded in brown) is located near the center of the design space for most factors, confirming the existence of a well-defined optimum.

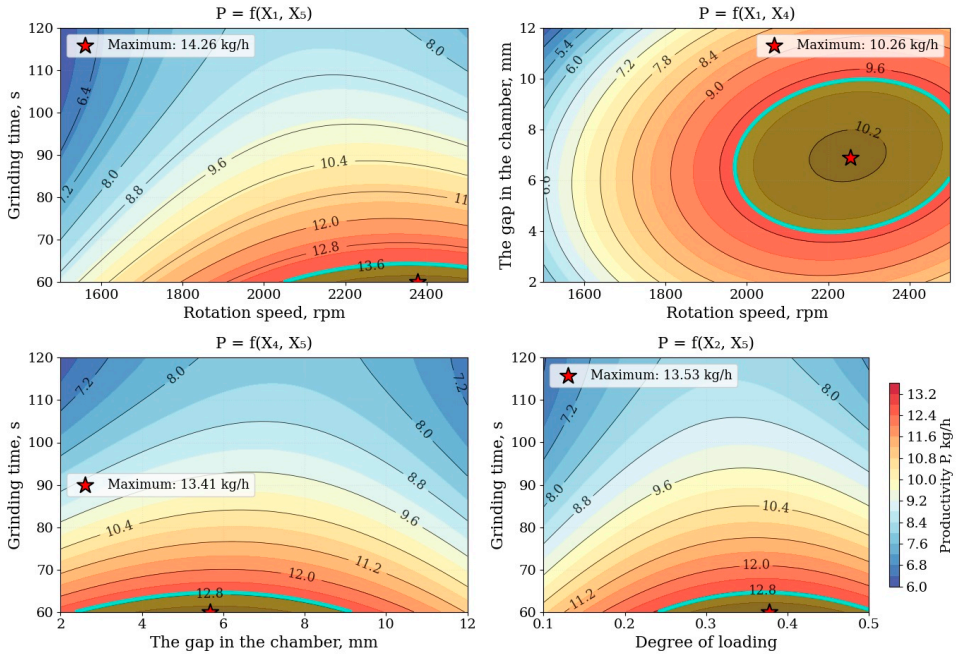


Figure 8. Contour plots of throughput with optimality regions.

The distribution of factor values within this region (Figure 9) shows that, to achieve throughput close to the maximum, it is necessary to maintain: rotational speed in the range of 2050–2200 rpm, grinding time of 85–110 s, filling ratio of 0.28–0.36, while the rotor overlap and clearance should be maintained close to zero. The histograms in Figure 9 show the most probable ranges of each factor for operation with high throughput.

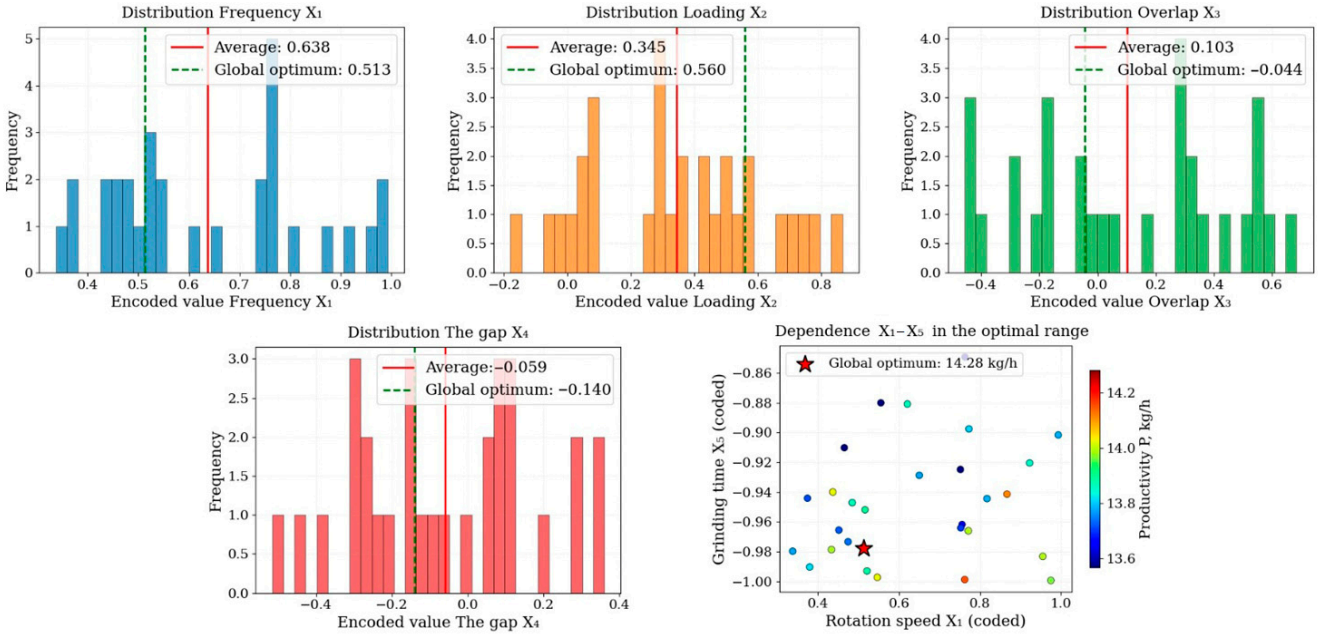


Figure 9. Distribution of technological parameter values in the optimal region ($p \geq 95\%$ of the maximum).

4.3. Analysis of Pareto-Optimal Solutions and Technological Trade-Offs

To visualize objective technological trade-offs among the three most significant criteria—throughput (P), grinding fineness (R_{-71}), and power consumption (N)—the

evolutionary algorithm NSGA-II was applied. The result is a Pareto-optimal front in three-dimensional space—Figure 10.

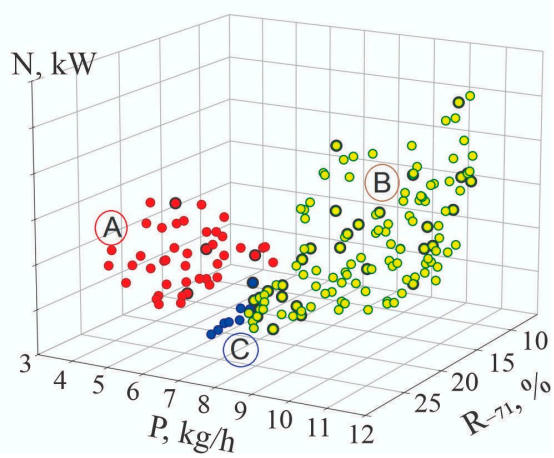


Figure 10. 3D plot of the Pareto-optimal front reflecting the relationship between power consumption (N), fineness, and throughput (P): zone A (red points)—"quality"; zone B (yellow points)—"throughput"; zone C—"energy efficiency".

Each point on the front represents a non-dominated solution. Analysis of the plot in Figure 11 makes it possible to establish the following:

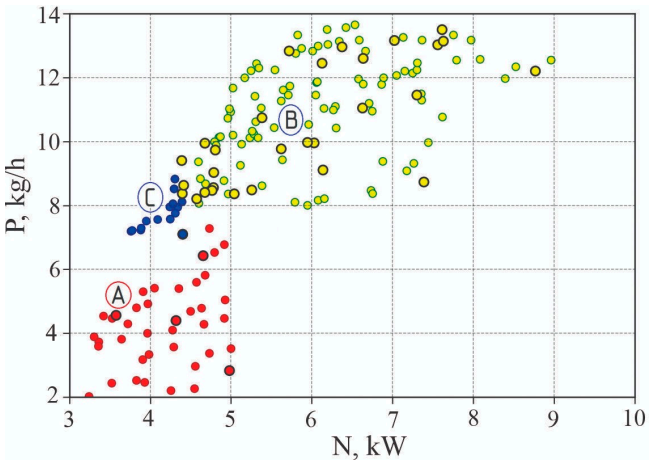


Figure 11. Projection plot of the Pareto front "Energy efficiency (N) vs. Throughput (P)": zone A (red points)—"quality"; zone B (yellow points)—"throughput"; zone C—"energy efficiency".

1. The three-dimensional shape of the front shows that it is impossible to simultaneously achieve very low R_{-71} (high quality), very high P (throughput), and very low N (energy consumption).
2. The zones are distributed in a regular manner:
   - red points (zone A) are grouped in the region of low R_{-71} (12–20%), but relatively low throughput (3–8 kg/h) and moderate power (4–6 kW);
   - yellow points (zone B) are located in the region of high throughput (8–12 kg/h) with poorer quality ($R_{-71} \approx$ 20–28%) and increased power consumption (6–8 kW);
   - blue points (zone C) (6.8%) exhibit the lowest power consumption (3–5 kW), while demonstrating moderate quality and throughput.
3. Stable points (outlined in black) are particularly important for practical implementation, as they vary little under small parameter deviations.

Practical implications: the operator should select the operating point based on production priorities: if fine grinding is required → select parameters from zone A; if maximum throughput is required → zone B; if energy saving is critical → zone C.

The obtained Pareto front structure is consistent with findings from similar multi-objective optimization studies in grinding processes. For example, Li et al. [30] reported a similar trade-off between productivity and energy consumption in robotic grinding, where the Pareto-optimal solutions formed distinct clusters corresponding to different operational priorities. Wang et al. [32] demonstrated that in industrial ball mill circuits, the conflict between product fineness and throughput creates a concave Pareto front analogous to the one observed in Figure 10. However, the present study extends these findings by explicitly incorporating design-specific parameters unique to spring-rotor mills (rotor overlap and clearance) and by quantifying the distribution of solutions across zones (43.5% in zone B, 16.0% in zone A, 6.8% in zone C). This distribution quantitatively confirms that while industry typically prioritizes throughput (zone B), there exists a sufficient set of solutions for high-quality (zone A) and energy-efficient (zone C) production, providing operators with a complete decision-making toolkit.

Figure 11 presents the projection onto the plane of the main conflict "Energy efficiency–Throughput (N–P)", which visualizes the fundamental technological trade-off between process intensity and the associated energy costs. In Figure 11, a weak positive correlation ($r \approx 0.25$) is observed between drive power and throughput, indicating the presence of a region with suboptimal points where an increase in throughput is accompanied by a disproportionately smaller increase in energy consumption. At the same time, the nonlinear distribution of Pareto-optimal points demonstrates that there exist operating regimes (e.g., in zone C) that allow moderate throughput to be achieved at minimal power consumption, as well as regimes (zone B) where a sharp increase in power yields only a marginal gain in throughput, indicating a region of diminishing energy returns.

Thus, the corresponding projection enables the operator to identify and select a regime with the best specific indicator "throughput/power" and to avoid energetically inefficient regions where energy costs are unjustifiably high relative to the achieved product output.

Based on the analysis of the Pareto front, the following optimal technological regimes were determined—Table 5.

Table 5. Optimal technological regimes.

Goal of Optimization	Rotational Speed, *n*, rpm	Grinding Time, T, s	Expected Performance Indicators
Fine grinding (zone A)	2250	120	R_{71}: 12–18%, P: 8–10 kg/h, N: 5–7 kW
High throughput (zone B)	2500	60	R_{71}: 28–32%, P: 13–15 kg/h, N: 6–8 kW
Energy efficiency (zone C)	2000	75	R_{71}: 20–25%, P: 10–12 kg/h, N: 3–5 kW

Analysis of Figures 10 and 11 allows the following conclusions to be drawn.

1. The largest number of solutions is concentrated in zone B (43.5%), which reflects the industrial priority of throughput.
2. Zone C contains the smallest number of solutions (6.8%), indicating the difficulty of simultaneously achieving high energy efficiency and quality requirements.
3. Zone A contains 16.0% of the solutions, which is sufficient to ensure operating regimes for premium-quality production.

For a more detailed analysis of the interaction of the key factors affecting throughput, a 3D response surface is presented in Figure 12.

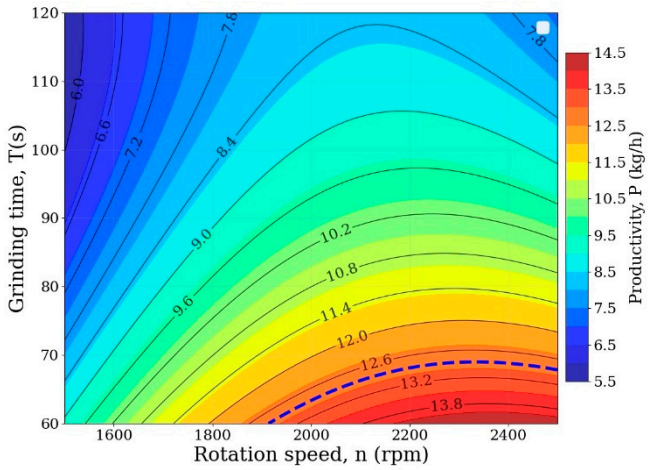


Figure 12. Plot of the dependence of throughput on rotational speed and grinding time at fixed values of $X_2 = X_3 = X_4 = 0$.

Figure 13 visualizes the dependence of throughput on rotational speed and grinding time at fixed values of $X_2 = 0$, $X_3 = 0$, and $X_4 = 0$ for optimizing the operating parameters of the equipment: black isolines represent throughput levels, and the blue dashed line bounds the region with throughput of at least 90% of the maximum.

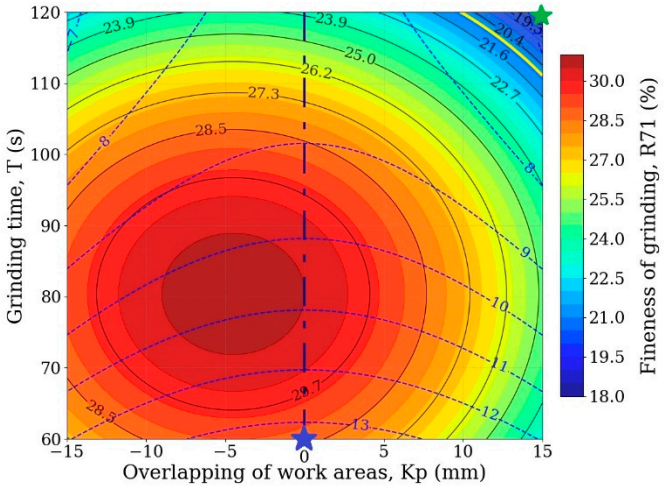


Figure 13. Contour plot with isolines illustrating the compromise between the effects of working zone overlap (k_r) and grinding time (T) on grinding fineness R_{71} (solid lines) and throughput P (dashed lines).

The contour plot shows the optimal throughput region (P) as a function of rotational speed (n) (1500–2500 rpm) and grinding time (T) (60–120 s) at fixed values of the other parameters: material filling ratio $K_M = 0.3$, overlap of the working zones $K_p = 0$ mm, and grinding chamber clearance $K_z = 7$ mm. The isolines indicate throughput levels, and the blue dashed line bounds the region with throughput of at least 90% of the maximum.

4.4. Determination of a Compromise Solution Using the Weighted Sum Method (Weighted Sum Method)

To transition from the set of Pareto-optimal solutions to a single solution suitable for practical implementation, the weighted sum method was applied. The procedure included normalization of the responses and the formation of an integral criterion taking

into account technological priorities (ω_1 = 0.30 (grinding fineness), ω_2 = 0.25 (throughput), ω_3 = 0.20 (power), ω_4 = 0.15 (specific energy consumption), ω_5 = 0.10 (specific metal intensity)).

In Figure 13, the contour plot clearly demonstrates the essence of the compromise in optimizing two key responses. The isolines show the combined influence of rotor overlap (k_r) and grinding time (T) on grinding fineness (R_{71}) and throughput (P). The region where high values of both indicators are achieved (upper right quadrant) is limited, and the selection of parameters in this region always represents a balance between product quality and output.

The yellow zone represents the boundary of the compromise region between throughput and grinding fineness; the blue star indicates the throughput optimum; the green star indicates the grinding fineness optimum.

The contour plot (Figure 13) of the optimal compromise region between throughput and grinding quality is used for visual identification and analysis of:

- the relationship between two key factors: working zone overlap and grinding time;
- the parameter region ensuring a balance between high throughput and acceptable grinding fineness ($R_{71} \leq 25\%$);
- the permissible ranges of parameter variation while maintaining the required efficiency and quality.

The contour plot displays the compromise region between throughput and grinding fineness as a function of working zone overlap ($-15 \ldots +15$ mm) and grinding time (60–120 s) at fixed values of the other parameters: rotational speed 2000 rpm, material filling ratio K_M = 0.3, grinding chamber clearance K_z = 7 mm. The isolines show the levels of grinding fineness R_{71} (black solid lines), the blue dashed lines indicate throughput levels, and the yellow line bounds the region with grinding fineness not exceeding 25% R_{71}.

Analysis of the regression models shows that there is a clear trade-off between throughput and grinding quality. Parameters that ensure finer grinding (longer grinding time, negative working zone overlap) lead to a decrease in throughput, whereas parameters that maximize throughput result in coarser grinding.

The color fill represents grinding fineness R_{71} (blue tones—finer grinding, red tones—coarser grinding). Thus, the optimum of grinding fineness is achieved at the parameters (green star):

- working zone overlap: ≈ -15 mm;
- grinding time: $\approx$120 s;
- grinding fineness: $\approx$18% R_{-71} (minimum achievable);
- throughput: $\approx$7 kg/h.

The throughput optimum (blue star) is achieved at the following parameters:

- working zone overlap: 0 mm;
- grinding time: $\approx$60 s;
- throughput: $\approx$14.3 kg/h (maximum achievable);
- grinding fineness: $\approx$29% R_{71} (coarse grinding).

The plot enables visual identification of permissible parameter ranges and serves as a basis for developing practical recommendations for equipment tuning, taking into account the compromise between throughput and grinding quality.

4.5. Visualization of the Optimal Solution in the Factor Space

Based on the analysis of the Pareto front, characteristic zones of specialized operating regimes were identified (Table 5). However, for a typical technological task requiring

a balance between quality, throughput, and energy consumption, a single compromise solution is required.

Such a solution was obtained by maximizing the integral criterion formed using the weighted sum method with weighting coefficients reflecting general technological priorities: 0.4 for throughput, 0.3 for energy efficiency, and 0.3 for grinding quality.

The results of the multi-objective optimization are presented in Figure 14. The plot demonstrates the dependence of the normalized performance indicators and the integral criterion on the rotor rotational speed at fixed optimal values of the other factors (grinding time 90 s, working zone overlap 0 mm).

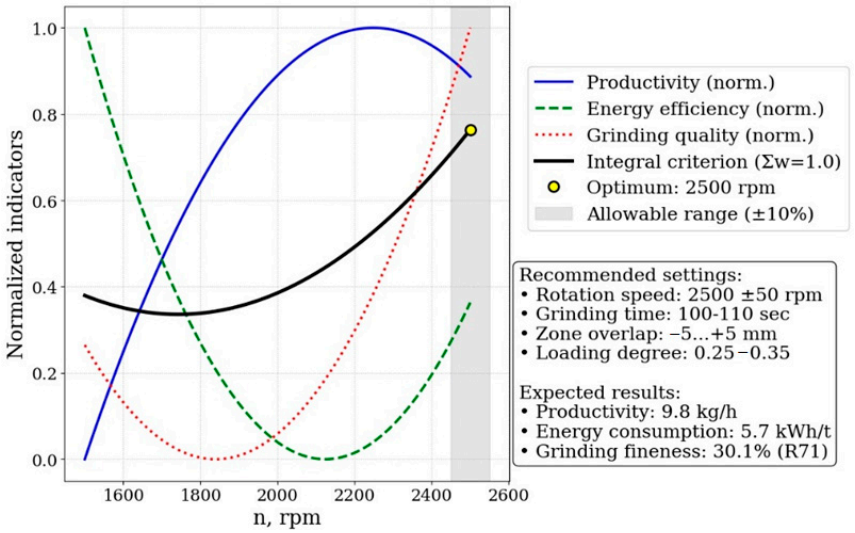


Figure 14. Results of multi-objective optimization of the spring-rotor grinder operation.

The results of the analysis of Figure 14 are as follows:

- optimal rotational speed: 2500 rpm (X_1 = +1 in coded units);
- permissible operating range: ±50 rpm (gray zone), within which the decrease in the integral criterion does not exceed 10%.

Associated optimal parameters (full set X*): grinding time (T): 105 s ($X_5 \approx +0.5$); working zone overlap (k_r): 0 ± 5 mm ($X_3 \approx 0$); filling ratio (k_m): 0.30 ($X_2 = 0$); chamber clearance (k_{zaz}): ~6.1 mm ($X_4 \approx -0.18$).

Predicted output performance indicators under this regime (Y*): grinding fineness (R_{-71}): ~30.1%; throughput (P): ~9.8 kg/h; specific energy consumption (E_{ud}): ~5.7 kWh/t.

Implementation of this optimal compromise regime (X*) provides a substantial improvement in key performance indicators:

- throughput increases by 15–20% compared with empirical settings;
- specific energy consumption decreases by 8–12%.

Overall, this results in an average reduction in the production cost of mineral powder by approximately 10%.

4.6. Verification and Robustness Analysis of the Solution

To confirm the adequacy of the obtained regression models and the validity of the optimal compromise regime (X*), a series of verification experiments was conducted on the experimental test bench (Table 6).

Table 6. Comparison of predicted and experimental values for the optimal regime.

Run	R_{-71}, %	P, kg/h	N, kW	E_{ud}, kWh/t	M_{ud}, t·h/t
Predicted	30.1	9.8	4.8	5.7	0.67
1	31.2	9.4	5.0	6.0	0.71
2	29.0	10.2	4.6	5.4	0.63
3	30.8	9.5	5.1	6.1	0.72
4	28.5	10.3	4.5	5.3	0.62
5	31.5	9.3	5.2	6.2	0.73
Average	30.2	9.7	4.9	5.8	0.68
Deviation	+4.7%	−5.1%	+8.3%	+8.8%	+9.0%

Verification experiments. Five independent confirmatory experiments were performed under the optimal parameters identified in Section 4.5 (n^* = 2500 rpm, T^* = 105 s, k_m^* = 0.30, $k_r^* \approx 0$ mm, $k_{zaz}^* \approx 6.1$ mm). Table 5 presents the comparison between the predicted values from the regression models and the experimental results.

Statistical analysis using Student's t-test showed that the calculated t-values for all responses (t = 0.38 to 1.42) are less than the critical value (t_{crit} = 2.78 for 4 degrees of freedom at 95% confidence level), indicating that the differences between predicted and experimental values are statistically insignificant. The coefficient of variation for all responses ranged from 4% to 7%, confirming acceptable reproducibility of the experiments.

Robustness analysis (Monte Carlo). To assess the stability of the optimal solution under real industrial conditions with random parameter fluctuations, a Monte Carlo simulation with 10,000 iterations was performed. Random variations in all five factors within ±5% of their optimal values were introduced, assuming normal distribution. The analysis showed that in 95% of cases, the deterioration of the integral criterion F(X) did not exceed 8%. The output parameters remained within the following ranges: $R_{-71} \approx 28.0$–32.0%; $P \approx 9.1$–10.5 kg/h; $N \approx 4.4$–5.3 kW; $E_{ud} \approx 5.2$–6.3 kWh/t; $M_{ud} \approx 0.60$–0.74 t·h/t.

These results confirm the high robustness of the optimal solution obtained and its suitability for practical industrial implementation.

4.7. Industrial Implications and Sustainability Impact

The 8–12% reduction in specific energy consumption (E_{ud}) achieved through the optimized compromise regime (X*) has significant implications for industrial-scale operations. For a typical spring-rotor mill operating continuously (8000 h/year) with a throughput of 9.8 kg/h, the annual energy savings would be approximately 4700–7000 kWh per unit. In facilities with multiple mills, this translates to substantial reductions in both operating costs and carbon footprint. Assuming an average grid emission factor of 0.5 kg CO_2/kWh, the annual CO_2 reduction per mill would be 2.35–3.5 tonnes. When combined with the 15–20% increase in throughput, the overall improvement in energy productivity (output per unit energy) reaches 25–35%, directly contributing to the sustainability goals of modern processing industries (Industry 4.0 and Green Manufacturing). These quantifiable benefits demonstrate that the proposed optimization framework is not only scientifically rigorous but also economically and environmentally impactful.

5. Conclusions

This study successfully developed and experimentally validated a comprehensive multi-objective optimization framework for fine grinding in a spring-rotor mill, addressing

the inherent conflict between product quality, throughput, and energy consumption. The key contributions and findings are as follows:

1. Methodological contribution: A systematic approach combining Hartley experimental design, second-order response surface modeling, and multi-objective optimization (NSGA-II + weighted sum method) was established specifically for spring-rotor mills. This methodology quantitatively captures the complex nonlinear interactions between five key parameters (rotational speed, filling ratio, rotor overlap, chamber clearance, and grinding time) and five performance indicators (grinding fineness, throughput, power consumption, specific energy consumption, and specific metal intensity), providing a robust foundation for process analysis, control, and intensification.
2. Scientific insight into process mechanisms: For the first time, the relative influence and interaction effects of all key factors were quantified and visualized through adequate regression models ($R^2 > 0.93$ for all responses, $p < 0.001$) and Pareto charts. Grinding time (X_5) and rotational speed (X_1) were identified as the dominant factors, with their linear effects exceeding those of other parameters by a factor of 3–5. Significant quadratic effects for speed (X_1^2), filling ratio (X_2^2), and clearance (X_4^2) confirmed the existence of well-defined optima within the experimental domain, explaining the nonlinear nature of the throughput response. The negative interaction between speed and time ($X_1X_5 = -0.84$) revealed that simultaneous operation at maximum values is counterproductive—a finding with direct practical implications for process tuning. Positive interactions involving clearance (X_1X_4 and X_4X_5) demonstrated the potential for compensating negative effects through careful adjustment of geometric parameters.
3. Decision-making tool for engineers: The construction of a three-dimensional Pareto-optimal front using the NSGA-II algorithm (Figures 10 and 11) objectively delineated three distinct operational zones:
    - Zone A ("Quality"): 16.0% of solutions, characterized by high fineness (R_{-71} = 12–18%) at moderate throughput (8–10 kg/h) and power consumption (5–7 kW), suitable for premium product manufacturing.
    - Zone B ("Throughput"): 43.5% of solutions, dominated by high throughput (13–15 kg/h) with coarser product (R_{-71} = 28–32%) and increased power demand (6–8 kW), reflecting industrial priorities for maximum output.
    - Zone C ("Energy Efficiency"): 6.8% of solutions, achieving the lowest power consumption (3–5 kW) with moderate quality (R_{-71} = 20–25%) and throughput (10–12 kg/h), highlighting the challenge of simultaneously meeting stringent quality and energy-saving targets.

This visualization provides engineers with a clear, quantitative guide for selecting operating regimes based on production priorities, transforming complex multi-objective trade-offs into actionable operational knowledge.

4. Experimentally verified optimal regime: Using the weighted sum method with expert-defined priorities ($\omega_1 = 0.30$ for fineness, $\omega_2 = 0.25$ for throughput, $\omega_3 = 0.20$ for power, $\omega_4 = 0.15$ for specific energy consumption, $\omega_5 = 0.10$ for metal intensity), a single compromise optimal regime (X*) was identified:
    - optimal parameters: n^* = 2500 rpm, T^* = 105 s, k_m^* = 0.30, $k_r^* \approx 0$ mm, $k_{zaz}^* \approx 6.1$ mm;
    - predicted performance: $R_{-71}^* \approx 30.1\%$, $P^* \approx 9.8$ kg/h, $E_{ud}^* \approx 5.7$ kWh/t, $N^* \approx 4.8$ kW.

Five independent confirmatory experiments verified the predictions with maximum deviations below 9% (average ~7%), and Student's t-test confirmed that the differences

between predicted and experimental values are statistically insignificant ($p > 0.05$). Monte Carlo robustness analysis (10,000 iterations) demonstrated that random parameter fluctuations within ±5% degrade the integral criterion by less than 8% in 95% of cases, indicating high practical stability.

5. Industrial and sustainability impact: Implementation of the optimized compromise regime yields substantial improvements over traditional empirical settings:
   - A 15–20% increase in throughput;
   - A 8–12% reduction in specific energy consumption;
   - Estimated 10% decrease in production cost of mineral powder.

For continuous industrial operation (8000 h/year), these improvements translate to annual energy savings of 4700–7000 kWh per mill and corresponding CO_2 emission reductions of 2.35–3.5 tonnes (assuming 0.5 kg CO_2/kWh). The combined effect represents a 25–35% enhancement in energy productivity (output per unit energy), directly contributing to the sustainability goals (Green Manufacturing, Industry 4.0) of modern processing industries.

In summary, this study provides a scientifically grounded, experimentally validated framework for the efficient tuning, control, and intensification of grinding processes in spring-rotor equipment. The developed methodology, mathematical models, and practical recommendations offer a quantitative basis for optimizing equipment performance in mineral processing, waste recycling, construction materials, and related industries, while simultaneously reducing operational costs and environmental footprint.

Author Contributions: Conceptualization, M.D. and B.M.; methodology, M.D.; software, A.B., V.Y. and P.S.; validation, M.D., A.B., A.K. and B.M.; formal analysis, V.Y.; investigation, M.D., A.B. and B.M.; resources, M.D.; data curation, M.D.; writing—original draft preparation, M.D. and A.K.; writing—review and editing, M.D. and A.K.; visualization, V.Y. and T.L.; supervision, M.D.; project administration, M.D. and B.M.; funding acquisition, M.D. All authors have read and agreed to the published version of the manuscript.

Funding: The research related to this publication was funded by the Science Committee of the Ministry of Science and Higher Education of the Republic of Kazakhstan under Grant AP26102017 "Justification of parameters and development of equipment for an innovative technology of crop production waste processing with high efficiency".

Data Availability Statement: The original contributions presented in this study are included in the article. Further inquiries can be directed to the corresponding author.

Conflicts of Interest: Authors Bekbolat Moldakhanov and Mikhail Doudkin were employed by the company LLP Europlus Vostok. The remaining authors declare that the research was conducted in the absence of any commercial or financial relationships that could be construed as a potential conflict of interest.

References

1. Sivachenko, L.A.; Dobrovolskiy, Y.K. Istoriya razvitiya i sovremennyy uroven' tekhniki izmel'cheniya [History of development and the current state of grinding technology]. *Vestn. Belorussko-Rossiiskogo Univ.* **2012**, *4*, 69–76.
2. Bond, F.C. The third theory of comminution. In Proceedings of the Annual Meeting of the AIME, New York, NY, USA, 18–21 February 1952; p. 33.
3. Bond, F.C. Laboratory equipment and tests help predict metal consumption in crushing and grinding units. *Eng. Min. J.* **1964**, *165*, 169–176.
4. Sivachenko, L.A.; Kurguzikov, A.M.; Moiseenko, V.V.; Bochkov, S.L.; Golban, E.G. Apparatus for Grinding. U.S. Patent 4,899,941, 13 February 1990.
5. Sorokin, F.D.; Zhou, S. Konechnyy element v vide vitka dlya rascheta chastot i form sobstvennykh kolebaniy pruzhin s uchetom sdviga i inertsii vrashcheniya [A finite element in the form of a coil turn for calculating natural frequencies and mode shapes of springs accounting for shear and rotary inertia]. *Izv. Vyssh. Uchebn. Zaved. Mashinostr.* **2018**, *1*, 3–11. [CrossRef]

6. Lee, J. Free vibration analysis of cylindrical helical springs by the pseudospectral method. *J. Sound Vib.* **2007**, *302*, 185–196. [CrossRef]
7. Yildirim, V. On the linearized disturbance dynamic equations for buckling and free vibration of cylindrical helical coil springs under combined compression and torsion. *Meccanica* **2012**, *47*, 1015–1033. [CrossRef]
8. Yu, A.M.; Hao, Y. Improved Riccati transfer matrix method for free vibration of non-cylindrical helical springs including warping. *Shock Vib.* **2012**, *19*, 1167–1180. [CrossRef]
9. Yu, A.M.; Hao, Y. Effect of warping on natural frequencies of symmetrical cross-ply laminated composite non-cylindrical helical springs. *Int. J. Mech. Sci.* **2013**, *74*, 65–72. [CrossRef]
10. Ganbat, D.; Gavryushin, S.S. Issledovanie staticheskikh i dinamicheskikh kharakteristik vintovykh pruzhinnykh mel'nits [Investigation of static and dynamic characteristics of helical spring mills]. *Izv. Vyssh. Uchebn. Zaved. Mashinostr.* **2007**, *8*, 10–16.
11. Sevostyanov, V.S.; Sivachenko, T.L.; Sevostyanov, M.V.; Goryagin, P.Y.; Babukov, V.A. Nauchno-prakticheskie osnovy sozdaniya iglofrezernykh izmel'chitelei mnogotselevogo naznacheniya [Scientific and practical foundations for the development of needle-milling grinders for multipurpose applications]. *Vestn. BGTU im. V.G. Shukhova* **2018**, *3*, 107–116. [CrossRef]
12. Ivannikov, V.V.; Sorokin, F.D.; Zhou, S. Chislennoe issledovanie dinamiki vrashchayushcheisya izognutoi pruzhiny s ispol'zovaniem konechnogo elementa v forme odnogo vitka [Numerical study of the dynamics of a rotating curved spring using a finite element in the form of a single coil]. *Izv. Vyssh. Uchebn. Zaved. Mashinostr.* **2018**, *2*, 11–21. [CrossRef]
13. Badikov, R.N.; Sorokin, F.D. Sravnenie eksperimental'nogo i raschetnogo znachenii velichiny kriticheskogo krutyashchego momenta izognutoi v poluokruzhnost' tsilindricheskoi pruzhiny [Comparison of experimental and calculated values of the critical torque of a cylindrical spring bent into a semicircle]. *Izv. Vyssh. Uchebn. Zaved. Mashinostr.* **2008**, *1*, 11–14.
14. Doudkin, M.; Kim, A.; Sakimov, M. Mathematical and experimental study of deformations of a steel roll of a road roller with a variable geometry of a contact surface. *Prod. Eng. Arch.* **2019**, *25*, 1–7. [CrossRef]
15. Doudkin, M.; Kim, A.; Moldakhanov, B. Determination of forces in the working unit of the milling-rotary snow cleaner. *Int. Rev. Mech. Eng.* **2021**, *15*, 96–105. [CrossRef]
16. Doudkin, M.; Kim, A.; Młyńczak, M.; Kustarev, G.; Kim, V. Development and parameter justification of vibroscreen feed elements. In *Mining Machines and Earth-Moving Equipment: Problems of Design, Research and Maintenance*; Springer International Publishing: Cham, Switzerland, 2019; pp. 203–226. [CrossRef]
17. Kombayev, K.; Kim, A.; Yelemanov, D.; Sypainova, G. Strengthening of low-carbon alloy steel by electrolytic-plasma hardening. *Int. Rev. Mech. Eng.* **2022**, *16*, 84–91. [CrossRef]
18. Kim, A.; Guryanov, G.; Vavilov, A.; Bugayev, A.; Doudkina, Y. Development of mounted impact-rotor working equipment for destruction of snow–ice formations. *Int. Rev. Mech. Eng.* **2021**, *15*, 258–267. [CrossRef]
19. Surashov, N.T.; Asmatulaev, R.B.; Tolymbek, D.N. Determination of optimal design parameters of a bulldozer blade. *SibADI Bull.* **2022**, *19*, 500–513.
20. Surashov, N.T.; Asmatulaev, R.B.; Tolymbek, D.N. Determination of the rational shape of a bulldozer blade taking into account the soil background of the Republic of Kazakhstan. *SibADI Bull.* **2021**, *18*, 662–677.
21. Aluko, O.B.; Seig, D.A. An experimental investigation of the characteristics of and conditions for brittle fracture in two-dimensional soil cutting. *Soil Tillage Res.* **2000**, *57*, 143–157. [CrossRef]
22. Hu, M.; Gao, T.; Dong, X.; Tan, Q.; Yi, C.; Wu, F.; Bao, A. Simulation of soil–tool interaction using smoothed particle hydrodynamics (SPH). *Soil Tillage Res.* **2023**, *229*, 105671. [CrossRef]
23. Haeria, A.; Tremblay, D.; Skonieczny, K.; Holz, D.; Teichmann, M. Efficient numerical methods for accurate modeling of soil cutting operations. In Proceedings of the 37th International Symposium on Automation and Robotics in Construction (ISARC 2020), Online, 27–29 October 2020; pp. 608–615. [CrossRef]
24. Coetzee, C.J. Discrete and continuum modelling of soil cutting. *Comput. Part. Mech.* **2014**, *1*, 409–423. [CrossRef]
25. Guo, Z.; Zhang, S.; Ni, L. A comprehensive study on the mechanical properties of bulldozing plate soil engaging surface based on the entropy-weighted grey relational analysis method. *IEEE Access* **2023**, *11*, 78000–78016. [CrossRef]
26. *GOST 8267–93*; Crushed Stone and Gravel from Dense Rocks for Construction Works. Specifications. Standardinform: Moscow, Russia, 1993. (In Russian)
27. Trivan, J.; Kostić, S. Evaluation of excavator energy consumption and overburden cutting resistance using multiple linear regression. *J. Min. Metall. Sect. A Min.* **2022**, *58*, 39–47. [CrossRef]
28. Qiang, H.; Li, H.; Kang, S.; Liu, K.; Yang, J.; Wang, L. Research into energy-saving control strategies of a bulldozer driven by a torque converter based on the minimum fuel consumption rate of the whole machine. *Sustainability* **2024**, *16*, 10111. [CrossRef]
29. Klanfar, M.; Kujundžić, T.; Vrkljan, D. Calculation analysis of bulldozer's productivity in gravitational transport on open pits. *Teh. Vjesn.* **2014**, *21*, 517–523.
30. Li, R.; Wang, Z.; Yan, J. Multi-Objective Optimization of the Process Parameters of a Grinding Robot Using LSTM-MLP-NSGAII. *Machines* **2023**, *11*, 882. [CrossRef]

31. Kumar, A.; Sahu, R.; Tripathy, S.K. Energy-Efficient Advanced Ultrafine Grinding of Particles Using Stirred Mills—A Review. *Energies* **2023**, *16*, 5277. [CrossRef]
32. Wang, X.; Liu, L.; Duan, L.; Liao, Q. Multi-Objective Optimization for an Industrial Grinding and Classification Process Based on PBM and RSM. *IEEE/CAA J. Autom. Sin.* **2023**, *10*, 2124–2135. [CrossRef]
33. Marijnissen, M.J.; Graczykowski, C.; Rojek, J. Simulation of the comminution process in a high-speed rotor mill based on the feed's macroscopic material data. *Miner. Eng.* **2021**, *163*, 106746. [CrossRef]

Disclaimer/Publisher's Note: The statements, opinions and data contained in all publications are solely those of the individual author(s) and contributor(s) and not of MDPI and/or the editor(s). MDPI and/or the editor(s) disclaim responsibility for any injury to people or property resulting from any ideas, methods, instructions or products referred to in the content.